Development of Ultra-Efficient Electric Motors

Final Technical Report

Covering work from April 2002 through September 2007

RELIANCE ELECTRIC COMPANY
26391 Curtiss Wright Parkway, Suite 102
Richmond Heights, OH 44143
(216) 261-3644 Fax (216) 261-3887

Date Published – May 2008

PREPARED FOR THE UNITED STATES DEPARTMENT OF ENERGY
Under Cooperative Agreement
No. DE-FC36-93CH10580

Disclaimer

Acknowledgements

The work described in this report has been the result of the efforts of a number of individuals from various organizations. The following people's direct contributions to the successful completion of this project are acknowledged. In many cases, these individuals provided insights and technical knowledge that resided in their listed organizations, as well.

Rich Schiferl - Editor

Reliance Electric
Boris Shoykhet
Andreas Meyer
Joseph Zevchek
Ellison Johnson
Michael Brinkmann
Michael Melfi
Michael Rubbo
David Driscoll
Donald Peterson
Viatcheslav Dombrovski
Debiprasad Panda
Clayton Rutti
Niel Widmer
Benjamin Hothem

Consultant
Stephen Umans

SuperPower, Inc.
Drew Hazelton

Oak Ridge National Labs
Christopher Rey
Robert Duckworth
Mike Gouge
Bill Schwenterly

National Institute of Standards and Technology
Ray Radebaugh

Table of Contents

List of Figures

List of Tables

1. Executive Summary

a. Project Scope

Electric motors utilize a large amount of electrical energy in utility and industrial applications. Electric motors constructed with high temperature superconducting (HTS) materials have the potential to dramatically reduce electric motor size and losses. HTS motors are best suited for large motor applications at ratings above 1000 horsepower (hp) [1], where the energy savings from the efficiency improvement can overcome the additional power required to keep the superconductors on the rotor cooled. Large HTS based motors are expected to be half the volume and have half the losses of conventional induction motors of the same rating. For a 5000 hp industrial motor, this energy savings can result in $50,000 in operating cost savings over the course of a single year of operation. Since large horsepower motors utilize (or convert) about 30% of the electrical power generated in the United States and about 70% of large motors are candidates for replacement by HTS motors, the annual energy savings potential through the utilization of HTS motors can be up to $1 Billion in the United States alone.

Research in the application of HTS materials to electric motors has lead to a number of HTS motor prototypes [2-6] yet no industrial HTS motor product has yet been introduced. These motor demonstrations have been synchronous motors with HTS field windings, on the rotor. Figure 1-1 shows a solid model rendering of this type of motor. The rotor winding is made with HTS coils that are held at cryogenic temperature by introducing cooling fluid from the cryocooler to the rotor through a transfer coupling. The stator winding is made of copper wire. The HTS winding is thermally isolated from the warm armature and motor shafts by a vacuum insulation space and through the use of composite torque tubes. The stator in Figure 1-1 is an air core stator in that the stator teeth and a small part of the yoke is made up of nonmagnetic material so the magnetic fields distribute themselves as if in air. Between the HTS field winding and the physical air gap is a series of concentric cylinders that act as vacuum insulation space walls as well as conducting paths for induced currents to flow in order to shield the HTS winding and the rotor cold space from time dependent fields. These time dependent fields may be caused by rotor hunting, during a change in motor load, or by non-fundamental component voltages and currents applied by the inverter. These motors are variable speed controlled by the inverter. Common large motor utility and industrial applications are pump and fan drives that are best suited by a variable speed motor. Inverter control of the HTS motor eliminates the need to design the rotor for line starting, which would dump a large amount of heat into the rotor that would then heavily tax the cryogenic cooling system. The field winding is fed by a brushless exciter that provides DC current to the HTS rotor winding. The stator winding is air or water cooled.

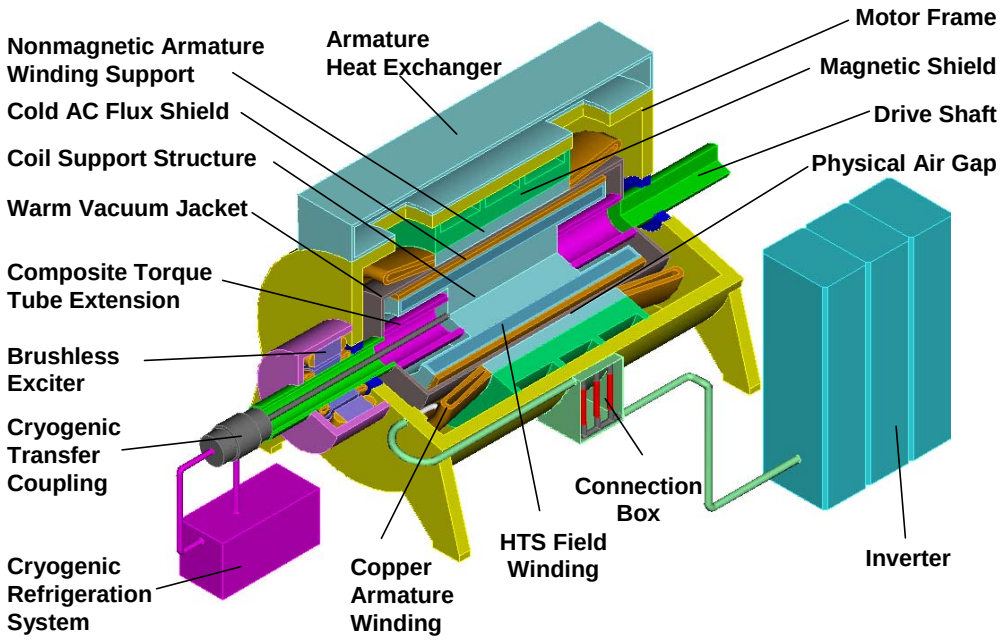

Figure 1-1: Synchronous motor with high temperature superconducting field winding and air core stator construction.

Technical and commercial hurdles to industrial HTS motor product introduction and customer acceptance include 1) the high cost of HTS wire and the cryogenic cooling system components, 2) customer concerns about reliability of HTS motors, and 3) the ability to attain the loss reduction potential of large HTS motors. Reliance Electric has demonstrated a number of HTS based electric motors up to a 1000 hp, variable speed synchronous motor [3,4] with an HTS field winding in the year 2000. In 2001 this motor was tested to 1600 hp with a sinusoidal (constant frequency) supply. Figure 1-2 shows the HTS motor on the dynamometer test stand in the Reliance Electric test lab.

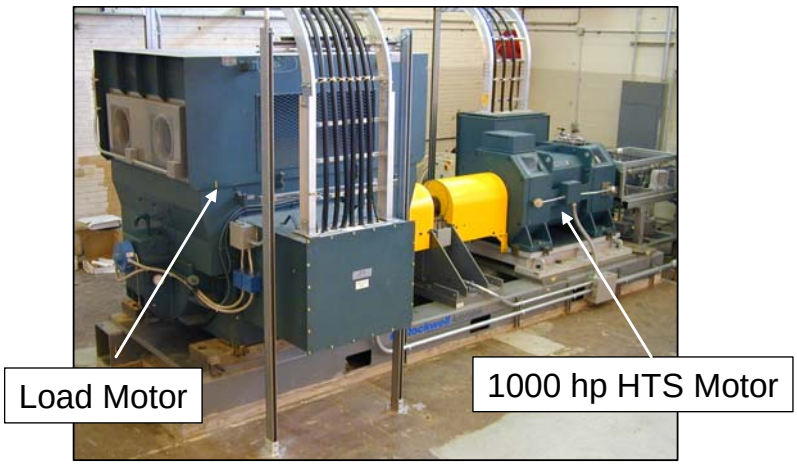

Figure 1-2: 1000 hp HTS synchronous motor on the test stand.

The extensive test program of the 1000 hp motor successfully demonstrated the technical feasibility of large HTS motors and the basic technologies involved, however the test results did indicate the need for design refinements. In addition, test results served to identify other more fundamental critical technology issues, and revealed the need to continue research efforts in order to improve future HTS motor first cost, reliability, and performance. The lessons learned from the development and testing of the 1000 hp motor were the basis for the tasks proposed for the project that is being described in this final report. These eight tasks and the technology and commercial issues they address are listed in Table 1-1.

Table 1-1: Research tasks for ultra-efficient HTS motor development

Research Task	HTS Motor Technology Issue	Commercial Viability Performance Driver
1.Eddy current heating in air core machines	High losses in the end regions of HTS synchronous motors with nonmagnetic stator winding support structure.	▪ Improved efficiency
2. Alternative superconducting motor topologies	Opportunity for reduced complexity or improved performance of HTS motors by inducing current in the HTS windings or the use of a combination of HTS windings and permanent magnets on the rotor and/or iron core stators.	▪ Improved efficiency ▪ Reduced cost
3. Alternative superconducting wire technology application	Lower first cost of HTS motors by utilizing lower cost second-generation HTS wire.	▪ Reduced first cost
4. Variable speed drive integration and rotor shielding	High losses in the rotor cold space due to inverter output current and voltage non-fundamental components.	▪ Improved efficiency
5. On-board cryogenic refrigeration system	Eliminate need for transfer coupling and stand-alone cryocooler for rotor cooling.	▪ Reduced first cost ▪ Improved efficiency ▪ Increased reliability
6. Coil quench protection system	Detection of quench (the phenomenon when an HTS coil transitions from superconducting to non-superconducting mode) and protection of HTS coils when quench occurs.	▪ Increased reliability
7. Composite torque tubes	Creep and fatigue of adhesive joints between the composite tube and metal flanges. Especially on the warm end of the tube.	▪ Increased reliability
8. Cryogenic persistent current switch for HTS windings	High heat leak into the rotor due to thermal conduction through the current leads for the HTS winding.	▪ Increased reliability.

b. Results Achieved

Project activity was completed for each of the eight research tasks listed in Table 1-1, including hardware demonstration of various components. Results, by task, are listed below.

Task 1: Eddy current heating in air core machines

- Three dimensional finite element modeling of the end region magnetic fields were used to identify the source of end region losses.
- A test rig was designed and built to investigate the impact of end region magnetic fields on losses.
- Test rig tests confirmed model results.
- Methods to nearly eliminate end region losses were determined.

Task 2: Alternative superconducting motor topologies

- Tests were conducted on permanent magnets to determine performance at cryogenic temperatures.
- HTS motors with induced currents in the HTS rotor windings were investigated and it was concluded that the synchronous motor topology with a field winding exciter (see Figure 1-1) is a better topology.
- Conventional, iron-core stator topologies were investigated and shown to be the optimal choice for HTS motors based on total cost of operation (first cost and operating cost).

Task 3: Alternative superconducting wire technology application

- The world's first motor utilizing second generation HTS conductor was demonstrated. This was a 7.5 hp motor with rotating second generation HTS field windings cooled with liquid nitrogen.
- Design studies of a large HTS motor with second generation HTS field coils were completed showing that HTS motors can be economically viable at HTS wire costs of $15 /kA-meter. Cryocooler costs become more of an issue at these HTS wire cost levels.

Task 4: Variable speed drive integration and rotor shielding

- Electromagnetic models of induced currents in air gap shields were developed and verified with test data.
- Electromagnetic models of HTS motors supplied by medium voltage (MV) current source or voltage source inverters successfully predicted high loss in the rotor cold space as observed during initial testing of the 1000 hp HTS motor.
- Proper warm shield design of the HTS motor rotor coupled with operating the inverter with the highest possible switching frequency can reduce the heat generated in the rotor cold space to a manageable level.

Task 5: On-board cryogenic refrigeration system

- A commercial, small capacity, pulse-tube cryocooler was integrated into a rotating test rig.
- Cryocooler performance was shown to improve (slightly) with rotation up to 1500 rpm. No cryocooler failure occurred during all rotating tests.

Task 6: Coil quench protection system

- Coupled electromagnetic, thermal, and electrostatic finite element modeling of quench in HTS coils were developed and applied to a number of first generation HTS coil topologies.
- Quench testing of a number of first generation HTS coils was completed and results verified the model predictions.
- A method to detect quench before damage occurs in the HTS field winding was developed and demonstrated.
- Results of wire, coil, and quench modeling were described in a series of technical papers that were presented in IEEE conferences [7-10].

Task 7: Composite torque tubes

- Creep tests were performed on various adhesives at elevated temperatures to determine creep characteristics for the bonded joint on the warm end of the torque tube.
- Creep test results confirmed the choice of an adhesive that will provide adequate life for the composite torque tube joints.
- Fatigue analysis of the composite torque tube system indicated that fatigue failure will not be an issue.

Task 8: Cryogenic persistent current switch for HTS windings

- A MOSFET based cryogenic persistent current switch was successfully demonstrated.
- Heat leak from the current leads for the HTS winding was estimated to be reduced by more than 90% using an HTS coil excitation system that has cryogenic persistent current switches.

c. Lessons Learned

The completion of these eight research tasks resulted in recommended design and control aspects of large HTS motors systems. In particular, future economically viable HTS motor systems will have:

- Rotating cryocoolers to reduce the rotor cooling system complexity and increase cooling system efficiency.
- Persistent current switches in the HTS coil excitation system to reduce heat leak into the rotor.
- HTS field winding geometry optimization to limit end region heating.

- HTS field coils systems (including proper cooling system and HTS conductor design) that avoid full coil quench with methods to detect the initial onset of pre-quench instability.
- Composite torque tubes with bonded joints that will not suffer from creep or fatigue failure.
- Iron core stators to reduce manufacturing and material costs.
- Warm air gap flux shields on the rotor to keep AC fields from reaching the HTS winding and eliminate rotor cold space heating.
- Current source inverters (CSI) drives with switching frequency above 400 Hz or voltage source inverter (VSI) drives with optimal switching patterns to reduce losses in the air gap flux shields.
- Second generation HTS wire to reduce cost. Wire costs must be at or below $15 / kA-m.

Economic viability of large HTS motors for utility and industrial applications is still dependent upon dramatic cost reduction of second generation HTS wire as well as dramatic cost reduction in cryocoolers that can provide cooling to 30 to 40 Kelvin. The relative complexity of an HTS motor compared to a conventional induction motor will continue to be a challenge for utility and industrial markets. The HTS motor's small size and increased efficiency provide tangible benefits that will drive these motors toward commercial success in some applications. However, the recent advent of permanent magnet motors provides a strong competitor to HTS motors for energy efficient large motor systems.

2. Program Management

a. Timetable, Tasks, and Deliverables

Project technical work spanned form April 2002 through September 2007. Project tasks were defined based upon a proposal submitted to the DoE in February of 2002 with the title: Research Topics for the Development of Ultra Efficient HTS Electric Motors. The eight project tasks that were proposed had specific deliverables associated with them. In some cases, project task deliverables were modified based on information learned as part of the research activities associated with the tasks. In all cases, final deliverables met or exceeded the initial deliverable goals. Table 2-1 lists proposed deliverables and actual deliverables for each of the eight tasks.

Table 2-1: Project deliverables by task.

Task	Deliverables from Proposal	Final Deliverables
1.Eddy current heating in air core machines	• Eddy current heating test apparatus • Final report	• Eddy current heating test apparatus. • Final report on eddy current heating modeling and test verification.
2. Alternative superconducting motor topologies	• Superconducting Induction Motor (SCIM) topology test apparatus • Hybrid superconducting / permanent magnet topology test apparatus • Final report	• Report on SCIM concept. • Report on permanent magnet performance at cryogenic temperatures. • Report on PM vs HTS motor design comparisons including option of stator magnetic teeth in both.
3. Alternative superconducting wire technology application	• Winding equipment to wind conductors supplied by vendors into coils • Second generation conductor coils • Final report	• Second generation conductor coils for a motor demonstration. • Report on 7.5 hp HTS motor with second generation HTS coils design and test. • Technical paper on HTS motor economics and applications. • Report on second generation wire performance characterization testing at ORNL.
4. Variable speed drive integration and rotor shielding	• Adjustable speed drive / shielding performance prediction model • Final report that describes methodology for resolving pertinent design and performance issues	• Report on air gap shield performance prediction model with comparison to tests of the 1000 hp motor. • Report on simulation models of various proposed solutions and best solution for future medium voltage (MV) motor systems. • Report on large horsepower superconducting motor performance when powered by a voltage source inverter (VSI) drive.
5. On-board cryogenic refrigeration system	• Rotating test apparatus • Pulse-tube cryocooler • Final report on cryocooler performance and model	• Rotating test apparatus. • Pulse-tube cryocooler. • Report on cryocooler performance in a rotating test rig and modeling results provided by NIST.

Task	Deliverables from Proposal	Final Deliverables
6. Coil quench protection system	• Quench protection system with performance verified through tests • Final report summarizing lessons learned and pertinent design issues	• Four technical papers published on quench modeling, quench testing, and HTS conductor performance modeling. • Quench protection system with performance verified through tests. • Final report summarizing lessons learned and pertinent design issues.
7. Composite torque tubes	• Torque tube test samples (for fatigue and creep) • Modified torsional test apparatus • Final report on test results and project activity	• Torque tube component test samples for creep testing. • Creep test apparatus. • Final report on creep test results and fatigue analysis.
8. Cryogenic persistent current switch for HTS windings	• Proof-of-concept persistent current switch (PCS) demonstration • PCS test apparatus • Final report on test results and conclusions	• Proof of concept PCS demonstration. • PCS test apparatus • Final report on test results and conclusions.

b. Program participants

Reliance Electric Company was the prime contractor for this project. Oak Ridge National Labs provided technical assistance through a Cooperative Research and Development Agreement (CRADA) related to quench testing and second generation HTS conductor performance testing. SuperPower, Inc. provided second generation HTS coils for the 7.5 hp motor demonstration. The National Institute of Standards and Technology (NIST) provided consultation on pulse-tube cryocooler performance modeling for the rotating cryocooler demonstration.

c. Program completion

The technical work and task technical reports were completed, under budget, by September 30, 2007. This final report completes the technical contractual requirements of this project.

3. Task 1: Eddy Current Heating in Air Core Machines

a. Task 1: Proposed Activities

One of the basic premises of superconducting motors is that they will be more efficient than conventional motors. Experimental results from the Reliance Electric 1000 hp HTS motor revealed significantly higher losses than anticipated. The excess loss above that which was initially predicted was about 1% of the rated motor output power. Thus, this problem impacts the efficiency of the motor and may make it difficult to reach the desired efficiency goals. Depending on the design details of the machine, these losses could almost offset the efficiency gains targeted for the HTS machine when compared to a conventional machine.

The air-core superconducting motor (see Figure 1-1) is different from a conventional motor in that it does not have any steel laminations in the stator slot area to direct and contain the magnetic flux. Without the steel core, the field is much higher in the winding support structures, end housings, bearing brackets, end laminations of the stator back-iron, and even the motor mounting structure. These higher AC magnetic fields have the potential to produce excessive eddy current losses in these parts of the motor.

The objective of this task was to determine the cause of extra losses in the end region of an air core superconducting motor and find ways to reduce or eliminate this type of loss. The approach taken was to 1) perform electromagnetic analysis of the magnetic fields and associated losses in the end region of an air core superconducting motor, 2) verify these models with tests, and 3) use the model to determine design rules to reduce or eliminate this type of loss.

b. Task 1: Results Achieved

Open circuit testing of the 1000 hp superconducting motor driven by another motor was used to determine the no load losses in the machine. Total no load losses (determined from the in-line torque transducer reading between the driving motor and the load motor) were ~14.7 kW. Losses due to windage and friction alone were ~1.4 kW so the stator core lamination and armature eddy current losses were ~13.3 kW. These losses were a combination of core loss and end region loss. Figure 3-1 shows the configuration of the core and end winding mechanical support structure for the 1000 hp motor. Open circuit tests were conducted with temperature rate-of-rise measurements in various parts of the end region of the motor in order to determine the loss distribution in the end region. Most of the end region loss was in the end plates and the winding support structure with about 20% of the loss in the lamination stack. Three dimensional electromagnetic FEA was conducted to estimate the end region losses. Figure 3-2 shows the eddy current components in the end region as calculated. Figure 3-3 shows the distribution of losses (both measured and determined from analysis) for the 1000 hp motor showing good correlation between the measured and calculated values. The loss in the end winding support structure and the end plates can be reduced by proper choice of materials and the

geometry of these support structures. The loss in the lamination stack needs to be better understood since the laminated core must be constructed out of electrical steel so a different material choice is not possible.

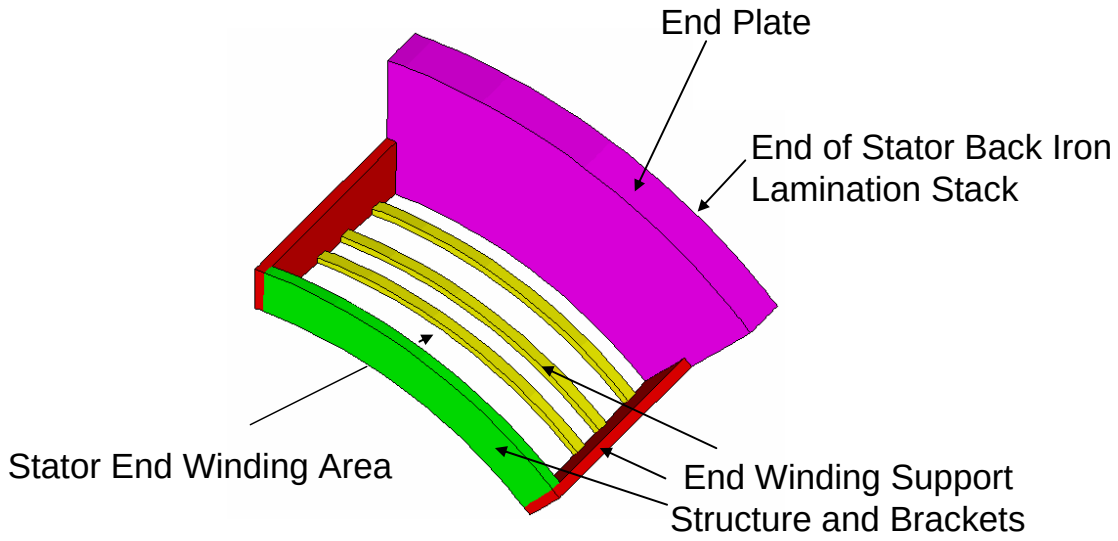

Figure 3-1: End region coil and core mechanical structural components for the 1000 hp HTS motor (1/16th of the circumference of the machine).

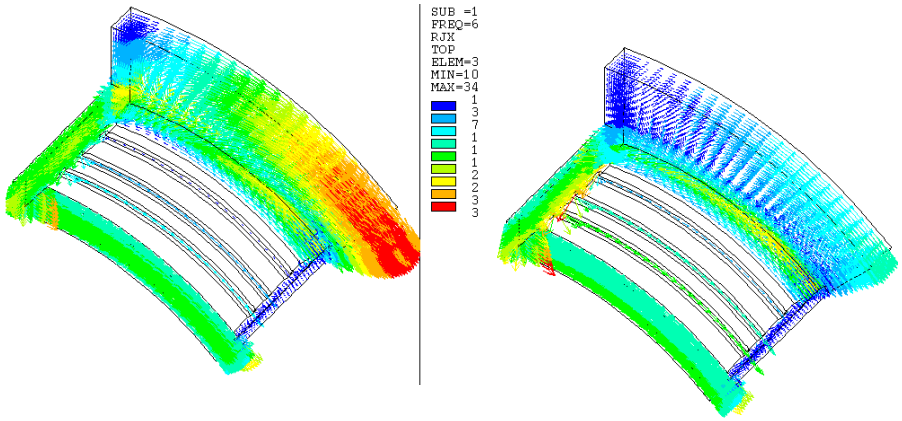

Real Component Imaginary Component

Figure 3-2: Calculated eddy currents in the end region of the 1000 hp motor.

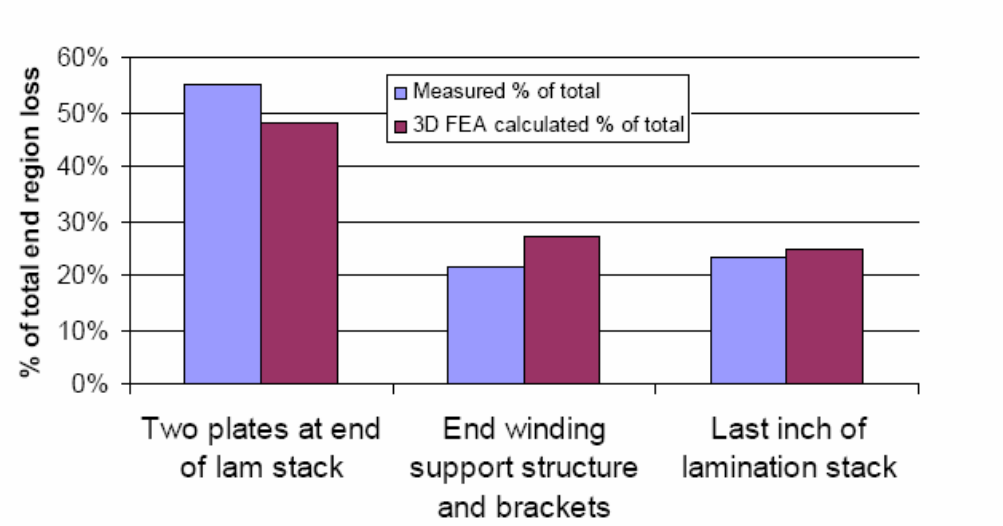

Figure 3-3: Calculated and measured loss components in the end region of the 1000 hp motor.

Loss reduction in the end region of the lamination stack is likely to depend upon the geometry of the motor and magnetic field pattern created by the HTS field winding. The loss calculation method used to get the data in Figure 3-3 for the last inch of the lamination stack was further verified for various field winding induced magnetic field patterns using the custom designed test rig shown in Figure 3-4. This rig used axially moveable permanent magnets to simulate the HTS field excitation. Tests were conducted for a variety of axial locations of the permanent magnets. Test results were compared to calculated results for various electrical steel excitation frequencies and magnet locations. Figure 3-5 shows comparison of measured and calculated losses for two different excitation frequencies and a range of magnet locations. The calculated loss matched test results very accurately. Results showed that for the proper choice of the axial location of the field excitation, the loss in the lamination end region can be dramatically reduced (more than a factor of 5 reduction compared to the worst case condition).

Figure 3-4: Test rig for verification of end region lamination stack loss calculations.

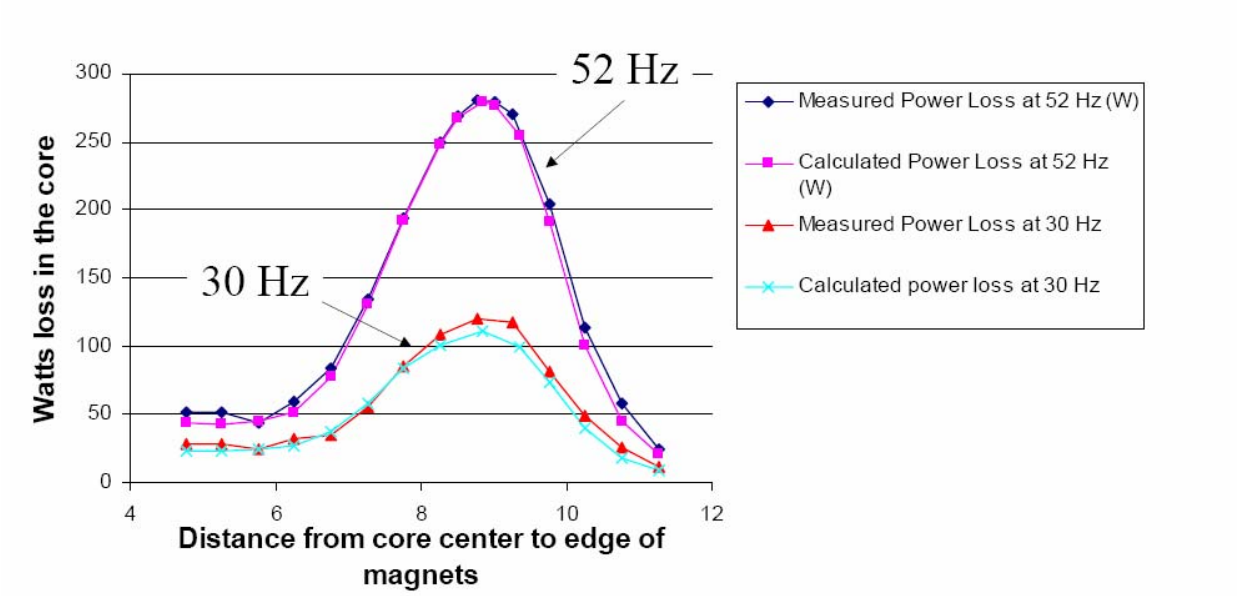

Figure 3-5: Test and calculated loss in the laminated core from the test rig.

c. Task 1: Conclusions

The source of extra end region loss for the air core, 1000 hp HTS motor was determined to be eddy currents in the end winding support structure and additional losses in the end region of the laminated steel. Three dimensional FEA modeling of these end region components successfully predicted the loss distribution in the end region as well as the loss as a function of motor dimensions in the laminated steel. Lamination steel losses calculations were verified through testing of a specially designed test rig. Methods to reduce (and nearly eliminate) the additional end region loss were determined and will be used for future air core HTS machinery designs.

4. Task 2: Alternative Superconducting Motor Topologies

a. Task 2: Proposed Activities

The Reliance Electric 1000 hp motor is a synchronous motor with HTS windings on the rotor providing field excitation. Field current is supplied by a brushless exciter, and cooling is supplied from a stationary cryocooler to the rotating field winding through a transfer coupling. Two alternative topologies were proposed in this task as potential improvements over the synchronous motor. These were a so-called superconducting induction motor (SCIM) and a combination superconducting and permanent magnet (PM) motor. The SCIM concept relies on the ability to induce current into the rotor winding, thereby eliminating the need for a rotor winding exciter and the associated heat leak into the rotor cold space due to the HTS winding current leads. The superconducting/permanent magnet motor design would utilize the HTS winding to magnetize and demagnetize the rotor mounted PM's and the PM's would add to the magnetic field created by the HTS winding. The advantage of this type of motor could be a reduction in the amount of HTS conductor (and its cost) in the motor as well as a controlled field capability for a PM based motor through the use of the HTS winding.

Both the SCIM and the HTS/PM motor concepts were evaluated by reviewing the principle of operation to determine technical viability and, if warranted, comparing their capabilities with the synchronous motor with HTS field windings on the rotor. In addition, an evaluation of an HTS motor with an iron core stator and rotor (in contrast to the air core construction of Figure 1-1) was conducted. An iron core motor should result in the need for less HTS conductor in the rotor, thereby reducing the cost of the motor.

b. Task 2: Results Achieved

The SCIM concept was evaluated based on information contained in two patents [11,12]. These patents describe a motor construction with HTS conductors on the rotor that allow current to flow near the surface of the rotor. Two possible methods to construct the rotor are to use HTS bars connected on the ends with HTS rings (like a squirrel cage in an induction motor) or using a thin film of HTS material on the surface of the rotor, like a conducting can. Both concepts rely on resistive currents in the rotor to start the HTS machine (like a conventional induction motor). Two possible methods to produce resistive current flow in the HTS windings are through the use of an applied magnetic field that exceeds the critical field of the HTS material or to apply selective heating to the HTS conductors to drive them above the critical temperature. The HTS windings are then caused to become superconducting by removing the magnetic field or removing the heat source. Once superconducting, it is proposed that current can be trapped in the HTS conductors on the rotor, allowing the motor to operate like a synchronous machine with a continuously flowing current.

After careful review of the proposed SCIM concepts several issues were identified that would make this type of machine impractical. These included:

1. The need to induce a large amount of loss in the rotor during the starting process would put a severe strain on the cryogenic cooling system for the rotor that would

make rapid transitions from the non-superconducting to superconducting state difficult to achieve.

2. The use of a thin film of HTS material on the rotor of a large machine to carry the required field excitation currents to operate the motor after the field windings transitioned to their HTS state would require a very large current density in the HTS material, larger than what may be possible with present-day HTS materials.
3. The fact that HTS conductors are not true superconductors in that they have a small amount of resistance, even when they are operating below their critical current, magnetic field, and temperature, would make sustaining an "induced" current in the rotor for an extended period of time impossible.
4. The fact that the SCIM topology does not eliminate or reduce the need for the cryogenic cooling system (in fact, it likely will result in the need for a larger capacity cryogenic cooling system to transition the rotor conductors from the non-superconducting to superconducting state) will result in the cost of this machine being too large for economic viability. Relative costs of HTS motor components are discussed further in Section 5 of this report where it is shown that the cryogenic cooling system costs are a significant part of the material costs of an HTS motor.

Based on these drawbacks of the SCIM concept, it was not further considered in this project task.

The viability of a combination of HTS and PM motor depends upon the optimum ratio of HTS- and PM-based magnetic field creation in the rotor. Choices include all HTS excitation or all PM excitation or some combination of the two. In order for the combination of HTS and PM excitation to make sense, readily available PM materials must be able to perform at cryogenic temperatures.

A simple test was conducted using Neodymium - Iron - Boron high field permanent magnets at cryogenic temperatures to see how they performed. Test results showed a 19% reduction in magnetic field strength at the surface of the magnets when the temperature was dropped from room temperature to 77 Kelvin. Although this is a significant drop, there still is a substantial amount of magnetic field created by the PM material at cryogenic temperatures so their use with an HTS winding can be considered. Based on these tests it appears that a combination HTS/PM motor is technically feasible. The economic viability of a combination HTS/PM motor depends upon the costs and benefits of HTS and PM materials in large industrial motors. Does it cost less to provide magnetic field excitation with HTS material or with PM material?

In order to investigate these costs, a design optimization study was conducted for a four pole, variable speed, 4500 hp industrial motor with either all HTS field windings or all PM rotor excitation. The optimization goals were to reduce the total cost of ownership of each motor over a two year period. For this study, cost of ownership included the first cost of the motor (related to material and component costs) and operating costs (related to motor energy savings due to efficiency improvement). The optimized HTS and PM

motors were found to be more efficient than an equivalent high efficiency induction motor of the same rating. HTS wire cost in the rotor were assumed to be $15 / kA-m at the operating field current and a temperature of 30 Kelvin. This is a cost level that second generation HTS wire is expected to reach in the future. The optimized PM motor used Neodymium - Iron – Boron permanent magnets at today's costs, when purchased in volume. The PM materials were assumed to be at normal rotor temperatures, not cryogenic temperatures, since this will result in a PM motor with the least amount of PM material to provide the required rotor excitation. The total cost of the PM material in the optimized PM motor was found to be twice as much as the total cost of the HTS material in the optimized HTS motor. Therefore, adding PM materials to the rotor of an HTS motor to reduce the amount of HTS wire will not reduce the cost of HTS material. At the future cost of HTS material it is likely that excitation using HTS wire will be less expensive than excitation using PM materials. In other words, if PM materials were added to the rotor of an HTS motor, the trade-off of reduction in HTS material cost with the added PM material cost would not be economically advantageous. The total material cost (HTS plus PM) would likely increase, especially in light of the fact that the PM material will operate a reduced performance at cryogenic temperatures. Therefore the combination HTS/PM motor does not make economical sense.

The third alternate motor topology considered in this task was a synchronous motor with HTS field windings and with magnetic steel (iron core) stator and rotor. Results of this evaluation will be presented in the next section where economic evaluation of HTS motors using second generation HTS wire is presented.

c. Task 2: Conclusions

Superconducting induction motors are not technically feasible. The high amount of heat generated in the rotor cold space during starting would be difficult to remove by the rotor cooling system. The ability to maintain a sufficient amount of rotor current during steady state operation (after starting) would be difficult due to the small amount of resistance that is present in HTS conductors, even when operating in their "superconducting" state.

The combination of HTS and permanent magnet excitation in a synchronous motor is technically feasible. However, the cost of HTS materials for rotor excitation (at $15/kA-m second generation HTS wire costs) will be less than the cost for permanent magnet materials for the same motor rating. Therefore, displacing HTS material with PM material in a combination HTS/PM motor does not make economic sense.

5. Task 3: Alternate Superconducting Wire Technology Application

a. Task 3: Proposed activities

All HTS motor demonstrations before the start of this project, including the Reliance Electric, 1000 hp synchronous motor with HTS field windings, used Bismuth-Strontium-Calcium-Copper-Oxide (BSCCO), powder in tube (PIT) HTS wire material and manufacturing technology. This wire technology has little hope of ever being available as a cost-competitive component of commercial industrial motors due to its high manufacturing cost and the large amount of silver that is required to construct the wire. Yttrium-Barium-Copper-Oxide (YBCO) coated conductor technology, the second generation (2G) HTS wire, shows promise of being significantly less expensive than the BSCCO PIT conductor and is likely to meet the performance requirements of HTS industrial motors. A description of BSCCO and YBCO conductor construction is included in [1].

The objective of this task was to investigate the use of 2G HTS material in industrial motors through 1) procurement of 2G HTS material and coils as they become available, 2) building test hardware to demonstrate the capability of taking 2G HTS wire and winding it into motor coils, and 3) conducting design studies using the properties and future costs of 2G HTS materials. The test hardware for this task included the demonstration of the world's first HTS motor using second generation HTS conductor. The design studies concentrated on design optimization of a 4500 hp, 1800 rpm industrial motor with 2G HTS field windings. The optimization goal was to maximize the two-year-cost-of-ownership-benefit (TYCOB) of this motor compared to a high-efficiency induction motor of the same rating. A two year payback on investing in high-efficiency motors is the typical time period used by industrial customers when making choices about high-efficiency motor purchases. Therefore, a positive TYCOB for the HTS motor would indicate economic viability of this motor for industrial applications. In addition, a technical paper describing the importance of second generation HTS wire for economic viability of HTS industrial motors was published [1].

b. Task 3: Results Achieved

A 7.5 hp synchronous motor with 2G HTS field windings was demonstrated. The objective of this small motor prototype construction and test was to show that 2G HTS wire can be successfully employed in applications involving rotating machinery and not to demonstrate the technology advantages that are expected to result from the second-generation HTS wire. As a result, this HTS motor was not built from "scratch". Rather, it was based on a standard 5-hp, 4-pole, 3-phase, 1800-rpm induction motor with the HTS synchronous rotor substituted for the original squirrel-cage rotor.

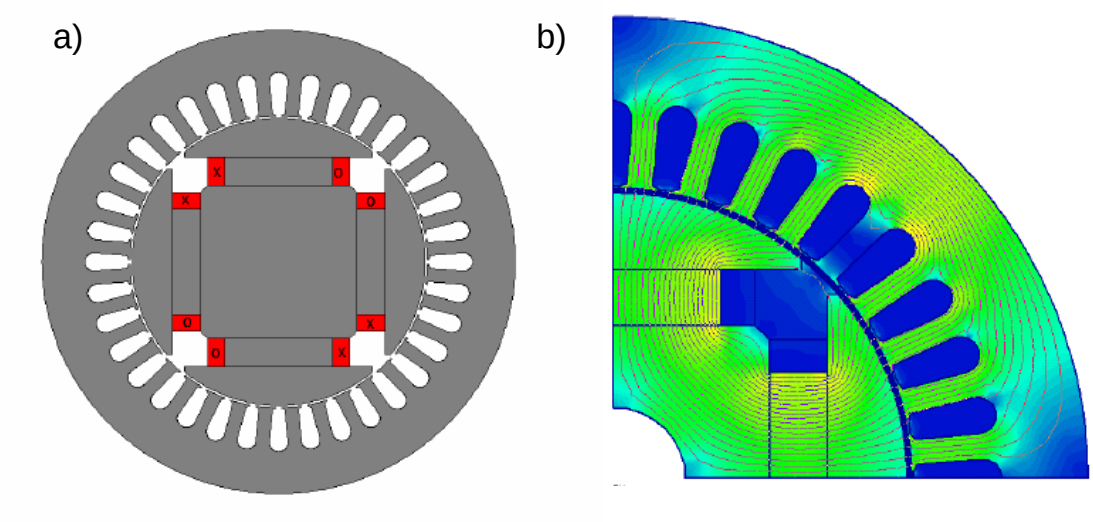

Figure 5-1: Rotor cross section of 7.5 hp HTS motor with 2G field coils. a) motor cross section with HTS field coil sides indicated as X and O, b) electromagnetic FEA flux plot for open circuit conditions.

Figure 5-1 shows an axial cross section of the resultant motor as well as the electromagnetic FEA based field solution for open circuit conditions. A salient-pole rotor configuration was chosen. The HTS coils are marked with 'X' and 'O' (to indicate different current directions). The rotor outer diameter was 12 cm. The motor had four second generation HTS coils supplied by SuperPower, Inc., see Figure 5-2. Each coil consisted of 25 turns of 1-cm wide superconducting tape with a total length of approximately 6 m of superconductor per coil. The cooling scheme for the motor consisted of liquid nitrogen flowing into the rotor via a bayonet inserted into a hole machined into the center of the opposite-drive-end rotor shaft extension. The liquid nitrogen then flowed out of the rotor into the air-gap, spilling over to the stator and out of the motor, ultimately forming a pool at the bottom of motor. A foam container, shown partially assembled in Figure 5-3, was used to contain the liquid nitrogen.

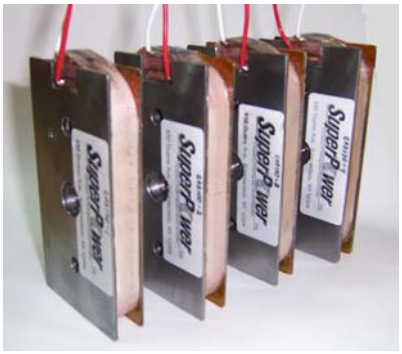

Figure 5-2: Four 2G HTS coils for the 7.5 hp motor demonstration.

Figure 5-3 shows the fully assembled motor and the motor under test. The motor was tested on a dynamometer stand driven by a variable-speed drive. Operating at a speed of 1800 rpm with a terminal voltage of 486 V and a current of 40 A in the HTS windings, the motor produced an output power of 7.5 hp (5.6 kW) during tests conducted in July of 2005. In addition, in the process of motor testing, the 2G HTS rotor coils was quenched a number of times without any resultant damage to the HTS coils showing the resiliency of this type of HTS coil. Further motor test information is given in [1].

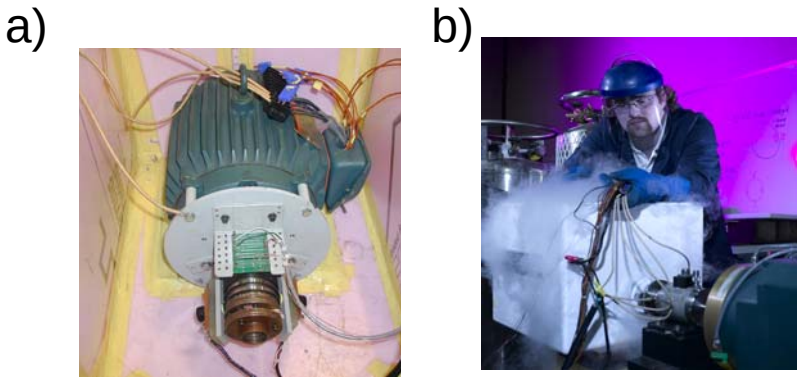

Figure 5-3: 7.5 hp motor with 2G HTS coils. a) motor in thermal isolation chamber with slip rings for rotor excitation in the foreground, b) motor under test with dynamometer load motor in the foreground.

Economic viability of large HTS motors using 2G wire was investigated through a design optimization study of a 4500 hp motor, four pole synchronous motor with 2G HTS field windings. The HTS motor was designed to maximize the TYCOB for the motor. This cost-of-ownership included the first cost of the motor (basically the expected sell price based on material and component costs and a reasonable profit margin) plus the input energy costs due to operation of the motor over a two year period of time. Energy costs were calculated assuming the HTS motor was operating at full load for 85% of the time over the entire two year period (24 hours a day, 7 days a week) and was off for the other 15% of the time. An energy cost of $0.07/kW-hr was used for this analysis.

The TYCOB was calculated by comparing the first costs and operating costs of the HTS motor to that of a high efficiency, 4500 hp, 4 pole induction motor. Maintenance and installation costs for the HTS motor and the induction motor were assumed to be equal for this economic evaluation. The 2G HTS motor optimization process involved calculation of motor cost and performance for a wide range of motor dimensions. Since HTS materials experience a small amount of loss, even in their superconducting state, the analysis included an estimate of the loss in the 2G HTS coils based on the required field current, magnetic field, and temperature for each motor design. Designs with too much rotor loss were eliminated from consideration since they would require too much cooling power to keep the rotor cool. Input power to the rotor cryocooler was considered as part

of the HTS motor loss and directly impacted its efficiency level. Designs were created assuming a 30 Kelvin HTS winding temperature and using 2G HTS wire with performance data for wire that would become available in early 2008. HTS wire cost was assumed to be $15 / kA-m at 30 Kelvin and a magnetic field level in the range of 2 to 3 Tesla.

All HTS motor designs were with an iron core rotor so magnetic steel was assumed to be utilized in the rotor coil support structure. This reduces the amount of HTS material needed to produce a given level of magnetic field in the motor air gap. Both air core and iron core stator construction were investigated. The iron core stator has magnetic teeth in the stator winding area and is the more conventional stator construction (similar to that of the baseline induction motor). The air core construction (as noted in Figure 1-1) has non-magnetic stator teeth and a magnetic back-iron ring behind the stator teeth for the return flux path. This air core construction requires more expensive copper Litz wire for the stator winding in order to reduce eddy current flow in the copper since the stator winding conductors experience the entire air gap magnetic field. In an iron core stator, the stator winding conductors experience only the slot leakage flux so Litz wire is not required. The additional cost of Litz wire was included in the air core HTS motor cost analysis. The goal of the HTS motor optimization was to find a design that would result in a positive TYCOB compared to the baseline induction motor, indicating economic viability of the HTS motor.

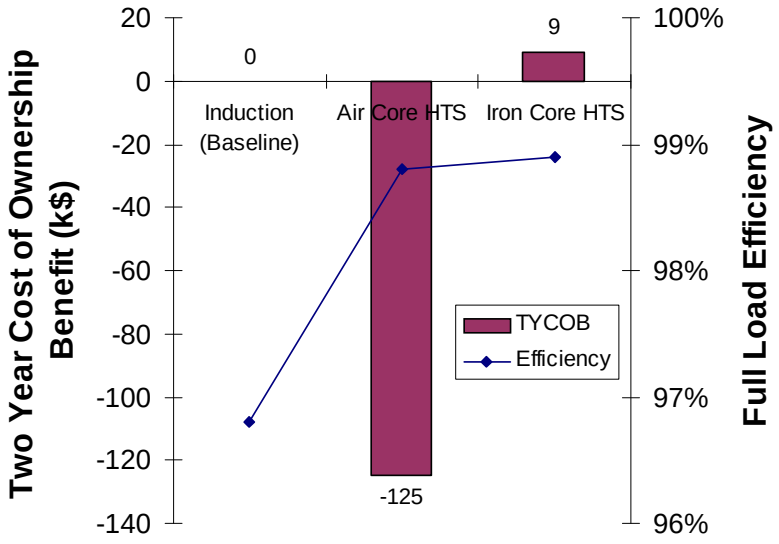

Figure 5-4: Results of cost of ownership optimization study for a 4500 hp, 2G, HTS motor.

Figure 5-4 shows the results of the optimization study for the 4500 hp motors. What is plotted is the TYCOB value for the motor designs with the highest value of TYCOB for each stator topology (iron core or air core). The optimum air core stator HTS motor has a

negative TYCOB compared to the baseline induction motor while the optimum iron core stator HTS motor has a positive TYCOB. The air core stator HTS motor is therefore not economically viable while the iron core stator machine is economically viable (based on future costs of 2G wire). Figure 5-5 shows a comparison of size and full load loss for the three 4500 hp motors. The HTS motors have about a third of the loss of the HTS motor and the iron core HTS motor is about one half the volume of the baseline induction motor.

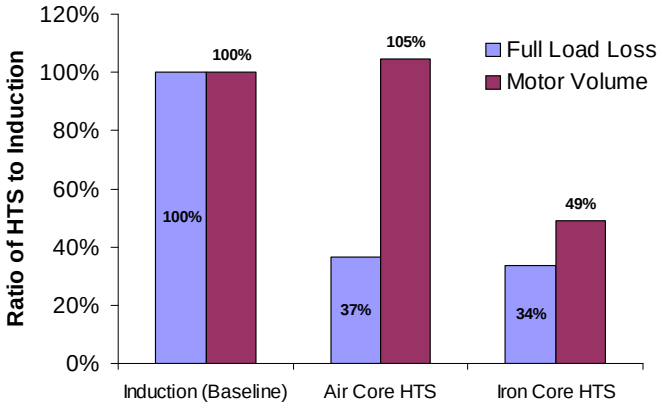

Figure 5-5: Size and loss comparison of 4500 hp motors.

Figure 5-6 shows the cost components of the various motors from the design optimization study. The multi-colored bars in this figure represent the key cost components that drive the first cost of the various motors. The pink bars marked "energy savings" for the two HTS motors indicate the money saved by the customer for two years of operation of the HTS motor compared to the induction motor based on the utilization and energy costs described earlier in this section. The two year cost of ownership is determined by moving up the multicolored bar representing the material cost (the first cost component) and then down by the amount of the pink bars (to subtract off the two year energy savings for the more efficient HTS motors). If the bottom of the pink bar is below the first cost level of the induction motor (the material cost component identified as Induction (Baseline) in the Figure) then the HTS motor has a positive TYCOB. The iron core HTS motor has much lower stator copper cost (by eliminating the need for the expensive stator Litz wire) as well as lower HTS cost, since less field winding excitation is needed with an iron core stator. The iron core HTS motor cryogenic system costs (cryocooler and transfer coupling) are a larger component of the first cost of this motor than the HTS winding cost. Cryocooler costs were assumed to be about half the cost of today's available cryocoolers for 30 Kelvin HTS coil operating temperatures. For example, a cryocooler that provides 80 watts of cooling at 30 Kelvin with an input power of 7 kW or less was assumed to sell for $15,000. This identifies the importance of reducing cryocooler system costs once HTS wire has reached cost levels projected (i. e. $15 / kA-m 2G HTS wire).

Figure 5-7 shows a comparison of the induction motor and the optimized 4500 hp HTS motor with iron core stator showing the size and performance advantages of the HTS motor. The HTS motor was constrained to have the same outer diameter as the induction

motor in order to provide a motor with the same shaft height. Volume reduction of the HTS motor was about 50% and loss reduction was over 60% compared to the induction motor.

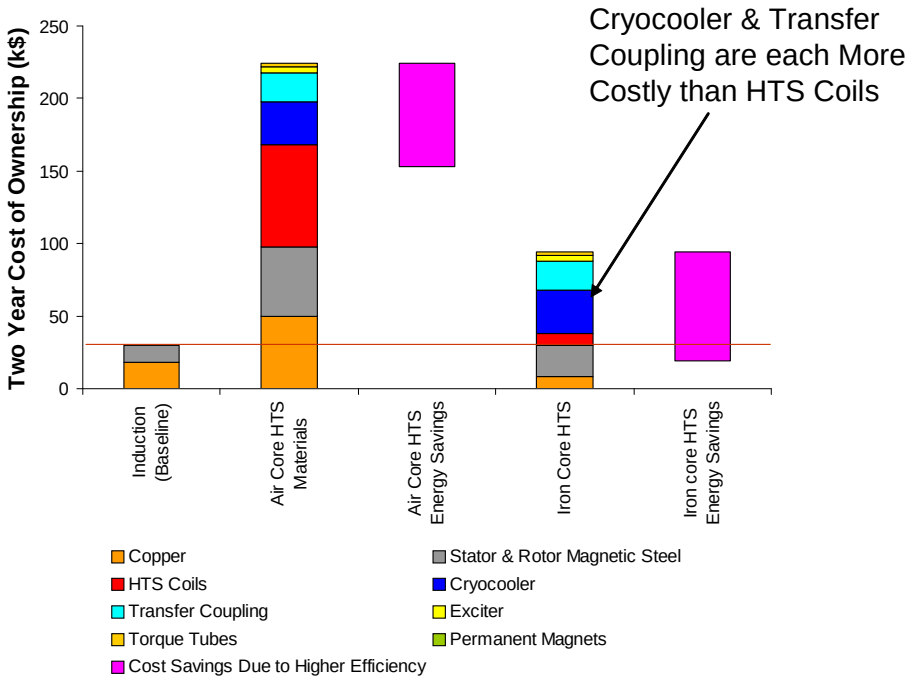

Figure 5-6: Cost of ownership components for 4500 hp induction and HTS motors.

Induction
96.8% Efficiency
64,900 in^3 Volume

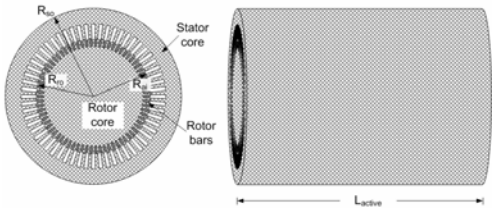

Iron Core Superconducting
98.9% Efficiency
31,900 in^3 Volume
2 Year TCO benefit = $9000

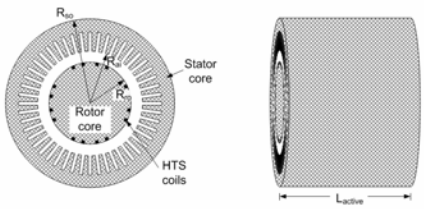

Figure 5-7: Optimum 4500 hp HTS motor design compared to the induction motor.

c. Task 3: Publications

A technical paper describing the advantages of HTS motors with second generation wire for industrial applications was presented at an IEEE conference [1].

d. Task 3: Conclusions

Affordable second generation HTS wire is key to the economic viability of HTS utility and industrial motors. Second generation HTS wire cost must drop to the range of $15 / kA-m at 30 Kelvin and 2 to 3 Tesla magnetic fields in order for HTS motors to be economically viable. In addition, cryocooler system costs must be reduced by at least a factor of two from today's sell price levels. A high reliability 70 watt, 30 Kelvin cryocooler with 7 kW input power (or less) is needed for future industrial motor applications for motors in the 5000 hp rating range and above.

Current second generation HTS wire and coil technology has progressed to the point where the demonstration of a 7.5 hp motor with second generation HTS coils could be done. This motor, the first one in the world to utilize second generation HTS coils, was successfully demonstrated in 2005.

6. Task 4: Variable Speed Drive Integration and Rotor Shielding

a. Task 4: Proposed Activities

Experimental results on the Reliance Electric 1000 hp HTS motor powered from a variable speed drive revealed that the drive current waveforms produced excessive loss in the rotor cold AC flux shield and the rotor cold space. For example, when the 1000 hp HTS motor was tested (in the year 2000) with a Current Source Inverter (CSI) medium voltage (MV) drive at 52 kW output and 600 rpm speed, rotor heating became excessive and motor testing was terminated. Temperature data taken during this test indicated an induced loss in the rotor cold space on the order of 35 watts. This is half the loss budget (70 watts) for the entire cryogenic cooling system for a large HTS motor. Determination of the cause of this high amount of loss and proposed methods to reduce this loss is the subject of this task.

Sensitivity to cold-space loss is a necessary but not sufficient indicator of operating problems. For example, the 1000 hp HTS motor was operated quite successfully when supplied from a 60 Hz, sine wave power system. Operating problems showed up when the motor was supplied by the CSI drive. While the 60 Hz sinusoidal voltages of the power system are relatively harmonic free, variable-frequency motor drives (whether CSI or Voltage Source Inverter (VSI) based) produce harmonic currents and voltages which in-turn produce asynchronous flux distributions in the motor. Because they are asynchronous, these fluxes induce eddy currents and produce dissipation in the rotor.

The approach taken to determine methods to reduce the loss in the rotor cold space when the motor is powered from a MV variable speed drive was to develop simulation tools that can predict the output current waveforms of the MV drive when it is powering the 1000 hp HTS motor. These current waveforms are then applied to a simulation model of the HTS motor that estimates the cold space induced currents and the cold space losses due to these non-sinusoidal current waveforms. Analysis was carried out for the CSI drive and results were compared to the 1000 hp motor system test data. Simulations tools were also developed for VSI MV drives for a typical VSI drive topology and control methodology. Finally, control methods to reduce the losses to acceptable levels in the HTS motor cold space were identified and proven through simulation models.

b. Task 4: Results Achieved

Transient simulation models of the 1000 hp motor fed by a CSI MV drive system were completed in order to predict the current waveform into the motor for various motor load conditions and drive operating conditions. The CSI drive system employs a capacitive filter between the output of the drive and the motor terminals as shown in Figure 6-1. The capacitive filter is required to eliminate large voltage transients at the motor terminals due to the discontinuous nature of the output currents from the CSI. The motor current waveforms obtained from the transient simulation were represented by a series of harmonic current components and these harmonic currents became the input to a rotor loss model that represented the rotor as a series of concentric shells of conducting material. For each stator time harmonic current applied (with the appropriate representation of the stator space harmonics based on the stator winding configuration),

the magnetic field distribution in space and time was determined for any configurations of these concentric shells that represented the warm AC flux shield, the inner (cold) rotor vacuum jacket, and the support structure for the HTS coils in the rotor cold space. In order to verify the loss calculation methods, tests were performed on the 1000 hp motor hardware with harmonic currents applied to the stator winding with a known conducting shell inside of the stator bore (see Figure 6-2).

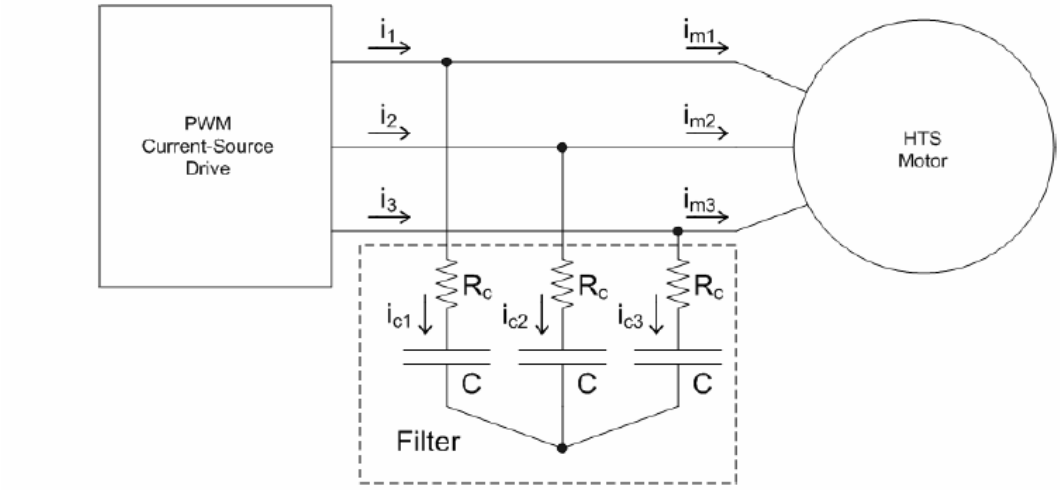

Figure 6-1: CSI driven HTS motor system that was used for testing the 1000 hp motor.

Figure 3: Photo showing the aluminum cylindrical shell in the 1000-hp stator.

Figure 6-2: Aluminum cylinder shell in the 1000 hp HTS motor stator bore.

Figure 6-3 shows a comparison of test results with the system shown in Figure 6-2 and calculated losses in the aluminum cylinder for a variety of applied stator currents and stator current frequencies. The model matches test data quite well over a wide range of frequencies and current levels.

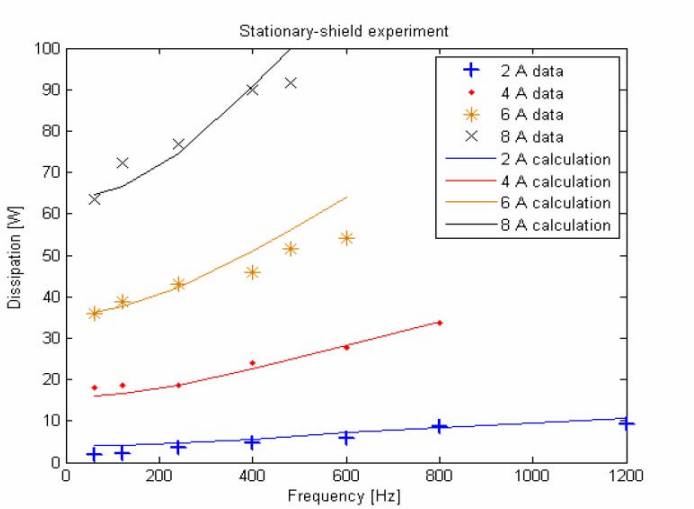

Figure 6-3: Measurements and calculated loss in a stationary aluminum shell inside of the 1000 hp motor stator.

The CSI drive chosen for the 1000 hp motor tests utilizes a technique referred to as selective harmonic elimination (SHE). Rotor heating test data from a motor operating point of 52kW output power at 600 rpm indicated a total rotor loss in the cold space of about 35 watts. A transient simulation of the 4-pole 1000-hp HTS motor at this operating speed and load and powered by a CSI with SHE control resulted in a current waveform as given in Figure 6-4. The simulated current data was input into the rotor loss calculation which predicted a rotor-cold-space power dissipation of 1.2 W and a power dissipation in the warm vacuum jacket of 54 W. In other words, the simulation methods under-predicted the loss in the rotor cold space since motor tests data implied 35 watts loss in the cold space. This is understandable, since not all of the details of the motor/drive system were fully simulated. For example, the DC link current was assumed to be constant, in reality it will have harmonic content that will contribute to the harmonic currents into the motor terminals. However, if the simulation results show excessive heating in the rotor cold space, then it is likely that this will be at least this bad in the actual motor/drive system. Figure 6-5 shows predicted loss in the rotor cold space for the 1000 hp HTS motor with the CSI drive for a range of motor speeds at rated output torque. Note that for many operating speeds, the cold space loss exceeds 50 watts and would result in excessive heating of the rotor. The jumps in predicted loss correspond to changes in switching algorithm of the CSI drive as the drive output fundamental frequency is varied. As the output frequency increases, the SHE algorithm becomes limited in its ability to eliminate harmonics due to a limitation in the maximum switching frequency of the drive switching devices. This results in higher harmonic content in the stator winding currents at higher motor speeds that translates into higher rotor losses. There are also electrical resonances that occur between the motor inductance and the drive filter capacitance that results in higher cold space losses at particular motor speeds.

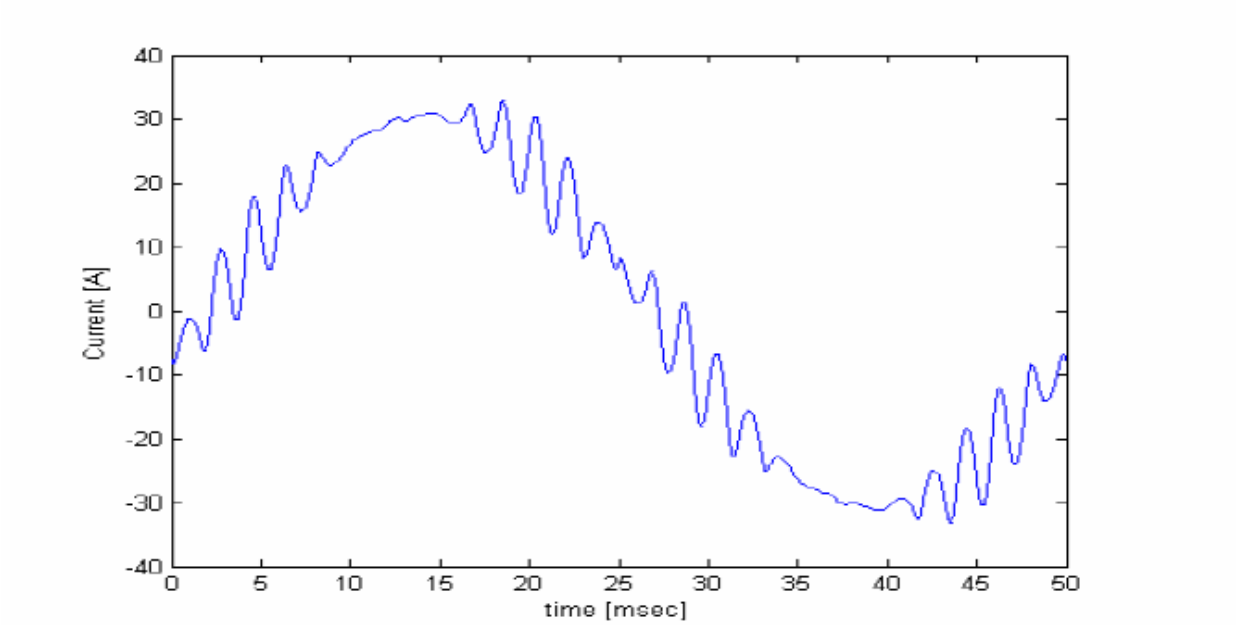

Figure 6-4: Simulated current waveform into the 1000 hp HTS motor at 600 rpm (20 Hz input frequency) and 52 kW output power.

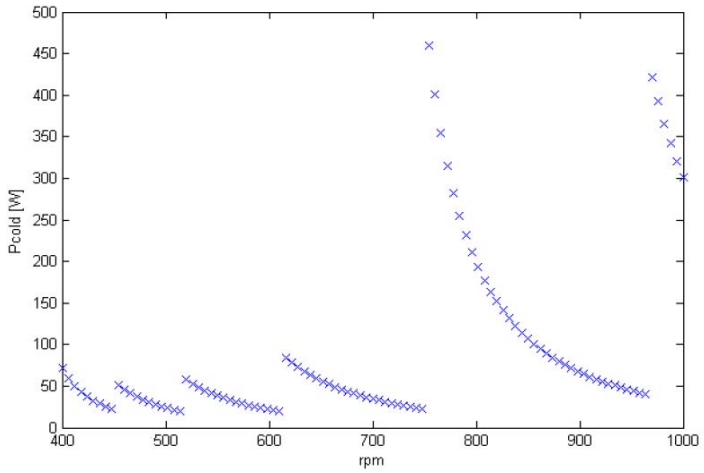

Figure 6-5: Simulated rated-torque, cold-space power dissipation over the speed range of 400 to 1000 rpm for the 1000 hp , four pole HTS motor fed by the CSI drive.

Various methods to reduce the cold space loss were considered, including modifications of the air gap flux shield system and modifications to the CSI drive and its control. Since the tests in the year 2000, CSI drive technology has advanced so that the PWM switching

frequency has increased by about a factor of two. This higher switching frequency results in the ability of the drive to reduce the harmonic current content over a wider fundamental frequency range, resulting in lower cold space losses. In addition, providing better AC flux shielding of the rotor by using a warm AC flux shield (assumed to be made of copper) at the outer vacuum jacket of the rotor will reduce the amount of harmonic fields that reach the rotor cold space. Figure 6-6 shows simulation results of cold space loss as a function of motor speed for a system with the higher CSI switching frequency and a warm AC flux shield. In addition, the CSI control was modified to obtain a better harmonic current reduction for this particular motor/drive system. Calculated cold space loss has been reduced to 10's of milli-watts (compared to hundreds of watts in Figure 6-5). It is expected that the calculation method underestimates the loss in the rotor cold space (as described above when results were compared to test data). However, even if the estimation is off by two orders of magnitude, the loss in the rotor cold space is capable of being handled by the rotor cooling system. Calculated loss in the warm AC flux shield for this design showed maximum warm space loss of less than 100 watts which will not create any cooling problems at the warm rotor surface.

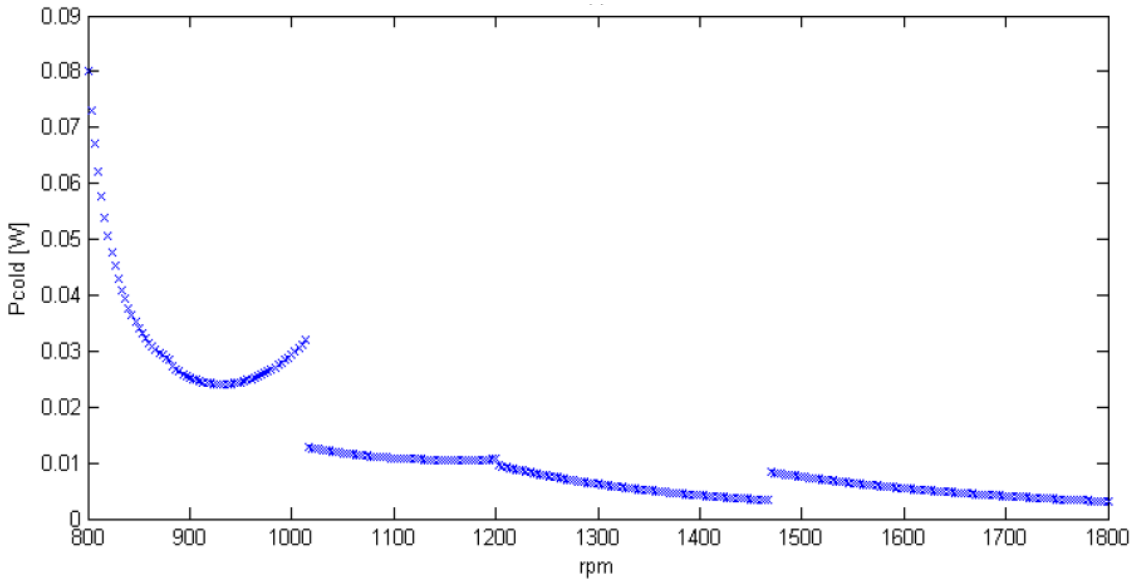

Figure 6-6: Simulated rated-torque, cold-space power dissipation over the speed range of 800 to 1800 rpm for the 1000 hp, four pole HTS motor with a warm AC flux shield and fed by the CSI drive with higher switching frequency.

An alternative MV drive topology for large horsepower motors is a VSI drive. Simulation results using a common, 3-phase, 9-level, cascaded H-bridge pulse-width modulated (PWM) voltage-source inverter feeding the 1000 hp motor were conducted. A time-step simulation of the motor/drive system resulted in predicted harmonic phase currents in the stator. These currents were used as inputs to the rotor loss model. Results

showed negligible loss in the rotor cold space with this motor/drive combination, even with the original rotor shielding configuration. One of the advantages the VSI system provides is the absence of a capacitive filter between the drive output and the motor terminals. This filter in the CSI system results in electrical resonance between the filter capacitance and the motor inductance that results in increased current harmonics at specific motor speeds that are difficult to mitigate without higher CSI switching frequencies or modifications to the motor rotor.

c. Task 4: Conclusions

Rotor cold space loss generation in the 1000 hp HTS motor is a result of time harmonic magnetic fields created by time harmonic currents in the stator winding when the motor is powered by a MV CSI drive. These losses were too large in the 1000 hp motor to allow successful operation of the motor with the CSI drive. Simulation of the motor/CSI system has successfully been used to characterize the loss in the rotor under a variety of operating conditions. These cold space losses can be reduced to acceptable levels by using a higher switching frequency CSI drive (which is now available) along with implementation of a warm AC flux shield on the outside of the rotor vacuum space. It has also been shown that use of a VSI drive with a common topology will result in acceptable cold space loss without rotor shield modifications.

7. Task 5: On-board Cryogenic Refrigeration System

a. Task 5: Proposed Activities

Transfer lines and transfer coupling losses significantly increase the overall cryogenic load to the rotor refrigeration system and hinder the system efficiency. Elimination of the transfer coupling will not only reduce approximately one quarter of the total cryogenic heat load, but also substantially increase system reliability. An on-board refrigeration system utilizing pulse-tube refrigeration technology offers a potential to achieve such a goal. This task involved investigation of the capability of using a rotating, pulse-tube cryocooler as a cooling method for the rotor. The approach taken was to purchase a small commercial pulse-tube cryocooler and integrate it into a rotating test rig to determine its capability while under rotation. In addition, a cryocooler expert at the National Institute of Standards and Technology (NIST) was contracted to provide a report on the expected performance of a pulse-tube cryocooler when rotated.

b. Task 5: Results Achieved

All superconducting rotating machinery demonstrations to-date included a stationary cryocooler and a system of delivery of the cryogen from the stationary frame to the rotating rotor. The delivery system included vacuum insulated transfer lines, a cryogenic transfer coupling with rotating seals, and piping inside of the rotor to deliver the coolant to the coils and return it back to the cryogenic transfer coupling. Obviously the concept of having the cryocooler right where it is needed, on the rotor itself, looks very attractive. The incorporation of a cryocooler into the rotor structure would allow making just one item-the rotor-instead of four items-the rotor, the transfer coupling, the transfer lines and the cryocooler. That would potentially decrease the cost of the HTS motor and increase its reliability. However, in the past, the topology of cryocooler compressors and other components absolutely was not suited for rotation and the concept of a rotating cryocooler seemed to be a complete fiction. The situation was changed when pulse-tube cryocooler technology was developed. The size and topology of this new device is such that it becomes possible to think about putting them into rotation.

There were two prime objectives of this task. The first objective was testing a pulse-tube cryocooler in rotation. This objective was achieved. The second objective was developing a rotating cryocooler performance model and compare the model results with experimental results. It was planned that the model would be developed by NIST and implemented by Reliance Electric. It was expected that this model would involve thermal-fluid modeling of the gas in the pulse-tube. However, in the process of developing the cryocooler performance model, Dr. R. Radebaugh of NIST concluded that for the chosen topology of the rotating pulse-tube cryocooler there is no expected adverse effect of rotation on cryocooler performance. Because of that, model development was limited to a thermodynamic analysis of the effect of rotation on the pulse-tube behavior, which did not require advanced fluid dynamics modeling.

The test rig that was designed and fabricated for the rotating cryocooler is shown in Figure 7-1. The chosen cryocooler unit was a model 2S102K made by the CFIC Company. The test rig was belt-driven using a variable speed motor to allow for rotation at a range of speeds.

The cryocooler cold head was instrumented with a temperature sensor and its load was provided by a small heater. The cold head of the cryocooler was enclosed by a vacuum space that was pumped out before the start of each rotating test. Sensor, instrumentation, and cryocooler power were provided through a set of slip rings mounted on the rotating shaft.

a) 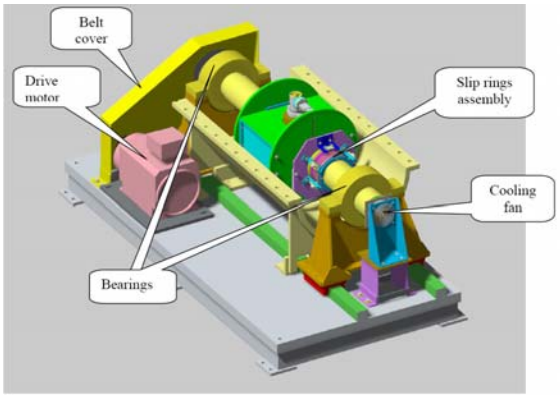

b) 

Figure 7-1: Rotating cryocooler test rig. a) Solid model rendering, b) Test rig under test with containment hood used for low speed testing.

Figure 7-2 shows test data at various rotational speeds for the cryocooler at two load points, zero heater power and 8 watts of heater power. For all speeds, up to 1500 rpm, the cryocooler performed well with no degradation in performance as the speed was increased. In fact, the cryocooler cold head was found to be slightly colder when it was rotated, compared to stationary operating conditions.

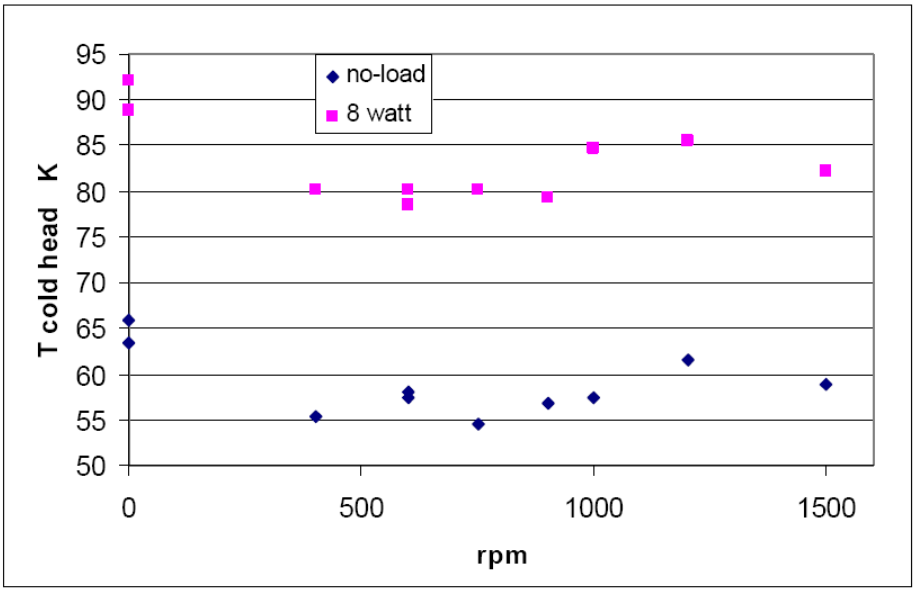

Figure 7-2: Measured cryocooler cold head temperature vs speed of rotation at two different cryocooler heat loads.

Tests were attempted above 1500 rpm but the test rig was found to have too high vibration to allow for testing at higher speeds. During one test attempt at 1800 rpm a instrument wire support bracket on the test rig failed. During this 1800 rpm test run, the cryocooler continued to perform without incident.

Modeling of the rotating cryocooler by NIST suggested that, for the orientation of the cryocooler in this test rig, the cryocooler performance should not be degraded when rotated. These model results matched the test data that was obtained.

c. Task 5: Conclusions

A pulse-tube cryocooler is suitable for usage in a rotating environment. The demonstrated test rig allowed testing to 1500 rpm. Above this speed vibration levels exceeded acceptable levels. The excessive vibration is believed to be a result of the large amount of asymmetry in the rotating system. This asymmetry is due to the fact that an off-the-shelf cryocooler was used in the experiment. A custom designed cooler system would eliminate this problem. There is no evidence that a pulse-tube based rotating cryocooler would not be successful at speeds exceeding 1500 rpm. Our belief is that the integration of the cryocooler into the rotor structure may be done for any rotational speed and such an integration will not increase the complexity of the rotor design.

A rotating cryocooler rotor cooling system provides the capability of hiding the cryogenic cooling system inside of the rotor. This feature will increase the probability of customer acceptance of HTS technology since nothing outside the motor would indicate that it is not a conventional motor. A rotating cryocooler cooling system results in the elimination of expensive components currently used for transferring the cryogen from the stationary cryocooler to the rotating rotor and back. These components are the cryogenic transfer lines, the cryogenic transfer coupling, and the piping routing the flow of the cryogen inside of the rotor. Another benefit of integrating the cryocooler into the HTS motor rotor is a substantial decrease of the heat load on the cryogenic part of the system since cooling can be applied directly to where it is needed on the rotor. The elimination of transfer lines and transfer coupling will also eliminate the heat leaks associated with these components.

Based on the test results presented here and the potential benefits of a rotating cryocooler to reduce the number of components in the rotor and to provide better cooling capability, a rotating cryocooler system development should be part of future HTS rotating machinery research activities.

8. Task 6: Coil Quench Protection System

a. Task 6: Proposed Activities

Stability of superconducting coils has always been a critical issue for the safe and reliable operation of superconducting devices. For large-scale HTS systems, it is imperative to understand the quench mechanism in order to prevent its occurrence and to mitigate its impact on the coil performance. Quench is a phenomenon that occurs due to thermal or flux disturbances that can lead to a local normalized zone. Without any detection and protective mechanism, a superconducting device could be easily destroyed by a quench. At the start of this project, technology in quench detection and protection for low temperature superconductors (LTS), typically NbTi and Nb_3Sn, was rather mature. Extensive research has lead to schemes that have been successfully applied to LTS conductors.

For HTS conductors, however, quench had not been a serious issue until recently when the critical current in HTS conductors and coils had reached levels for practical applications. Quench issues were addressed in the preliminary design of the HTS coils for the 1000 hp motor and measures were implemented in the final design for quench protection. Testing results from the 1000 hp HTS motor revealed that the protection mechanism for the HTS coils during motor transients was problematic. Voltage signals used for quench detection while the motor was operating had so much signal noise that the superconducting state of the field winding coils was almost impossible to monitor. In addition, during a routine test of one of the HTS coils for the 1000 hp motor the coil was permanently damaged (see Figure 8-1). This event occurred with little warning and was initially believed to be a coil quench.

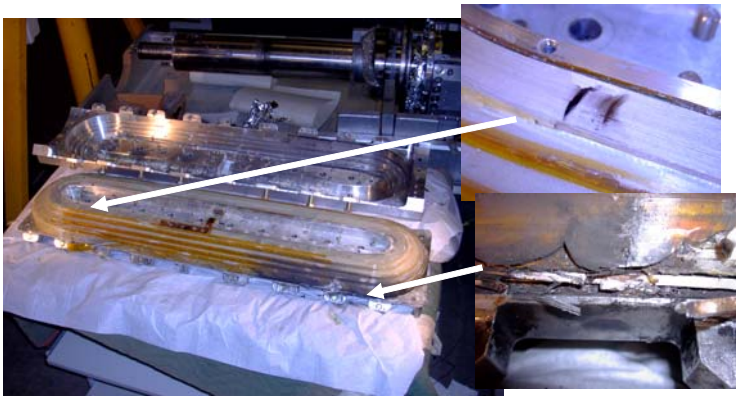

Figure 8-1: 1000 hp HTS motor coil showing damage after “quench” event.

This task investigated the quench phenomena associated with HTS coils with the objective of developing a reliable quench monitoring and protection system for field coils of HTS motors. The approach taken was to develop a modeling technique that characterizes the voltage, temperature, and magnetic field of an HTS coil during a quench event. Testing of a number of HTS coils (from the Reliance Electric 200 hp synchronous motor and the 1000 hp synchronous motor) was used to verify the model predictions and

to better understand what happens to the coil when conditions exist for a quench to occur. Coil testing was done at Reliance Electric and at Oak Ridge National Labs (ORNL) as part of a Cooperative Research and Development Agreement (CRADA). Finally, a reliable monitoring method to detect the potential onset of quench and prevent quench from occurring was devised and demonstrated through testing at ORNL.

b. Task 6: Results Achieved

Quench modeling and corresponding HTS coil test results are described in four technical papers that were the outcome of this task [7-10]. An overview of the test results and modeling activity is presented here followed by a discussion of the lessons learned in this activity.

Development of a computer simulation model of an HTS coil during a quench event was a key part of this task's technical activity. Before extensive modeling activity occurred, a review of published literature on HTS coil quench and quench modeling was conducted as summarized below.

Quench in HTS coils is the loss of superconductivity due to thermal instability. HTS conductors always have some very small but finite dissipation. This dissipation is a highly non-linear function of temperature and current. It also strongly depends on the magnetic field caused by the coil itself and by external sources. Thus the thermal conductivity equation governing heat distribution in the coil includes a heat source depending on the temperature, current and magnetic field. The presence of such a source creates the potential for thermal instability.

In LTS devices, thermal instability is typically initiated by small, randomly-distributed heat impulses associated with different dissipation mechanisms such as magnetic flux fluctuations, micro-cracks, tiny movements of the wire, mechanical hysteresis due to nominally-elastic loading-unloading cycles, small plastic deformations, and so on. These heat impulses are small and can cause quench only at low temperatures when the specific heat of the superconducting coil becomes very small. Since HTS devices operate at much higher temperature than LTS devices these factors do not play any role in the HTS quench phenomenon.

Our belief is that in rotating superconducting machinery there are three mechanisms that can initiate an HTS coil quench. The first mechanism will be referred to as a current induced quench. Current induced quench occurs when the current exceeds some value (I_q) and the cooling system is assumed to be in order and operating properly. The value of I_q is a system characteristic of the superconducting device including the cooling system. It was introduced in [13-18] and called the quench current. The second mechanism will be referred to as a thermally induced quench which happens at constant current due to a malfunctioning of the cooling system which could be due to refrigerator failure, vacuum problems and so on. In this case the temperature rises and at some point triggers a quench. The third mechanism is a joint problem, when a defective HTS wire joint heats the adjacent superconductor, raising the local temperature to the instability

region, or resulting in the instability of the joint itself; the later is possible because the resistance of a joint depends on temperature.

In this task, only the first two quench mechanisms, the current induced quench and the thermally induced quench, were studied. The joint induced quench is yet to be considered and is better studied when more data on the performance of high-current joints in HTS coils is gained.

The term "quench" was coined first for LTS devices and meant the formation and the propagation of a normal zone in a superconducting coil. For HTS materials the term "quench" is used in the same sense. Most of the focus of quench studies of HTS materials has been paid to normal zone propagation; the speed of the normal zone propagation was widely considered as "the key parameter that quantifies the quenching process in superconductors" (See [19], pp 1). It was found that the speed of the normal zone propagation in HTS tapes is very low compared with LTS devices. That was widely considered as the major problem for HTS quench detection and protection. The typical statement is as follows [20], pp.5: "The high thermal capacity of high Tc materials increases the difficulty of quench-detection, mainly because the quench-zone propagates very slowly in high-Tc superconductors....The results for BSSCO 2212 wires indicate at least one order of magnitude decrease in the speed of quench propagation, making it very difficult to detect the quench in a large coil. For active magnet protection, novel methods of quench protection and quench detection are required if the applications of high-Tc superconductors at high temperatures is to become a reality". In the course of the work performed on this task we came to the conclusion that low-speed propagation of the normal zone is not important for quench detection. This will be explained shortly. It is important for quench protection in the sense that passive protection is not possible, however, it does not affect the capability of developing active protection schemes. The perception about the importance of the normal zone propagation was inherited from LTS materials and misled many researchers, making them spend time and resources on excessive study of the normal zone propagation in HTS materials.

Another phenomenon, which is by far more important for quench detection and protection than quench propagation, did not get enough attention and had not been clearly defined. In this report we suggested the term "pre-quench instability" for this other phenomenon. It is during the pre-quench instability event that quench detection should be done. Design of the HTS conductor, coil, and cooling system to make the time spent in the pre-quench instability condition (before a quench occurs) long enough for detection, is very important for reliable operation of HTS coil systems.

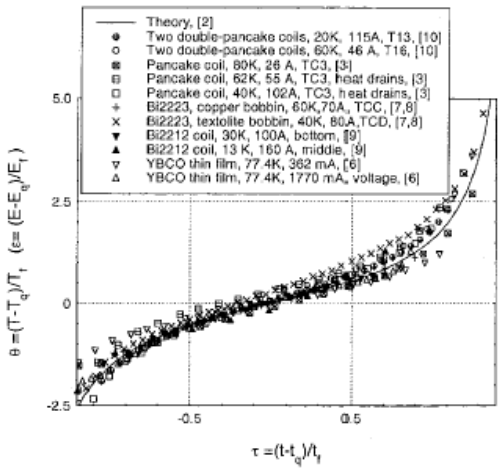

Figure 8-2: Dimensionless temperature (θ) and electric field (ε) versus dimensionless time (τ) for experiments with six different HTS devices.

Work on this task started from a literature study. Since the question of the speed of quench propagation dominated the literature on HTS quench, it was decided that it is necessary to learn how to implement Finite Element Analysis (FEA) simulations of quench propagation in HTS coils. When this process was completed it became obvious that some important link was missing in the whole concept. We were able to model quench propagation, to produce computer animations of the moving normal fronts, to obtain good correlations with the known analytical formulas for quench propagation speed, but we still did not know how to detect a quench and protect the coils.

The breakthrough in this project was started when we ran across a series of publications [13-18]. The research in these publications spanned about 4 years and was based on a significant number of experiments on quench of HTS coils. A very simple one-degree-of-freedom model of the coil quench was also proposed, which, with the proper tuning provided good correlation with the experiments. This model is called "The universal scaling law". Figure 8-2 shows the correlation of the experimental results with this theory. The major results of this work were summarized in the review [18]. The publications [13-18] provided a solid foundation for quench detection and protection in HTS devices.

One of the most surprising results of [13-18] was that the one-degree-of-freedom-model provided good correlation with experimental data. The model was based on the assumption that the temperature is uniform across the whole coil. This temperature was the only degree of freedom in the model. The simplest possible cooling model was used, namely, it was assumed that the heat removal rate for the whole coil is proportional to the difference between the coil temperature and coolant temperature. A single value of critical current was assumed for the whole coil. For some of the experiments in [13-18] these assumptions were approximately correct, but for the others they were not. For

example, the critical current strongly depends on the magnetic field and hence can not be the same across the coil even if the coil temperature is uniform. In one of our 200 hp HTS motor coils at 77 K the critical currents across the coil varied by a factor of 3.3 just due to the variation of the magnetic field. However, the accuracy of the one-degree-of-freedom model seemed to be the same for all tested coils. It seemed unbelievable that such a complex object as a superconducting coil can be presented by such a simple model.

The experimental work done as part of this task is described in [7], where current induced instability was studied. The HTS motor field coils were submerged into liquid nitrogen and the current was increased in small increments until instability was observed. The major difference between the experiments in [13-18] and [7] is that the coils used in our study were much larger. The other significant distinction of this project from this earlier research is our usage of much more complicated theoretical and computational tools. That enabled us to obtain new qualitative and quantitative results. Some of our results are in agreement with the earlier referenced work, but some are not. Our modeling includes the impact of the HTS conductor stabilizer for quench detection and protection while previous models do not include this affect. In addition, our modeling is able to distinguish between pre-quench instability and a true quench whereas the previously published work was largely related to the pre-quench instability phenomenon.

Testing of BSCCO HTS coils from the Reliance Electric 200 hp and 1000 hp motor field windings was conducted to better understand what happens to the coil voltage during a quench event. Figure 8-3 shows a typical voltage versus time curve for a liquid nitrogen cooled 200 hp motor field coil when the current is raised enough to cause the onset of a quench event. Note that there is a long time period (minutes in duration) where the coil voltage increases linear with time and then another rather long time period where the voltage starts to rise nonlinearly. Based on our understanding of the quench phenomenon, the entire time shown in Figure 8-3 is during pre-quench instability, before a true quench occurs. During repeated testing of the 200 hp and 1000 hp BSCCO HTS coils, it was possible to move in and out of the pre-quench instability region of operation without any damage to the HTS coils.

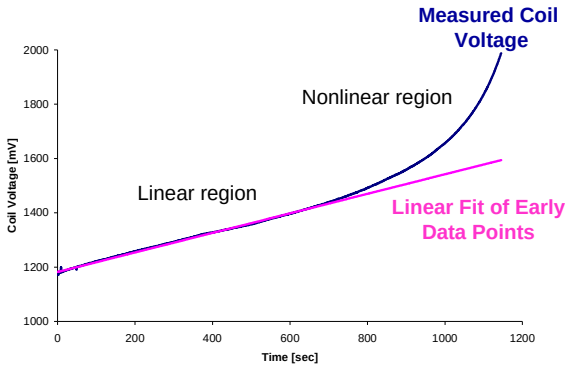

Figure 8-3: Typical test result for a constant applied coil current. Liquid nitrogen cooled 200 hp motor field coil with BSCCO HTS wire.

Figure 8-4 shows liquid nitrogen cooled test results for one of the 1000 hp, BSCCO, HTS coils. In this test, the coil current was stepped up from 30 to 32 amps in one amp increments. The quench current (I_q) for this coil with this type of cooling lies somewhere between 31 and 32 amps. Note that there is a considerable amount of time (hundreds of seconds) before the coil voltage begins to rapidly ramp up as the coil begins to transition from a pre-quench instability to a true quench somewhere beyond 500 seconds into this test.

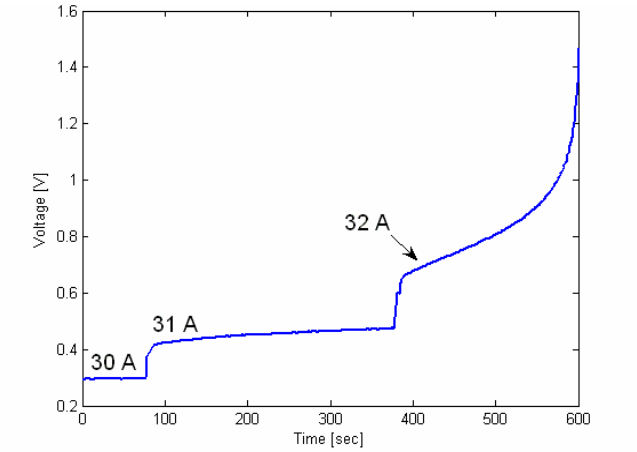

Figure 8-4: 1000 hp, BSCCO, HTS coil test with liquid nitrogen bath cooling.

Liquid nitrogen bath cooling tests were followed by conduction cooling tests at 30 Kelvin through collaboration with ORNL. Figure 8-5 shows the 200 hp and 1000 hp motor coils and the coil test fixtures that were fabricated for testing at ORNL. Testing was conducted with conduction cooling to mimic the type of cooling that is expected to be used in HTS motors. Cooling was provided by a thermally conductive path between a cryocooler cold head and the test coils. The 200 hp motor coils were tested as a pair (which allowed for various magnetic field loading based on excitation of a single coil or two coils) while the 1000 hp motor coils were tested one at a time. Figure 8-6 shows the 1000 hp HTS coil test fixture being lowered into the test chamber at ORNL.

200 hp motor coil

1000 hp motor coil

2 coils – mounted back-to-back

Coils Mounted in Test Fixtures for 30 K Testing

Single coil tested at a time

Figure 8-5: BSCCO HTS field coils and coil test fixtures for quench testing at ORNL.

Figure 8-6: 1000 hp HTS field coil being lowered into test fixture at ORNL.

Figure 8-7 shows test data at 30 Kelvin for a 1000 hp motor coil with various coil currents applied. The quench current (I_q) for this coil with this type of cooling is somewhere between 172.5 and 175 amps. Again, there is a considerable length of time (10's to 100's of minutes) during which the coil stays in the pre-quench instability regime.

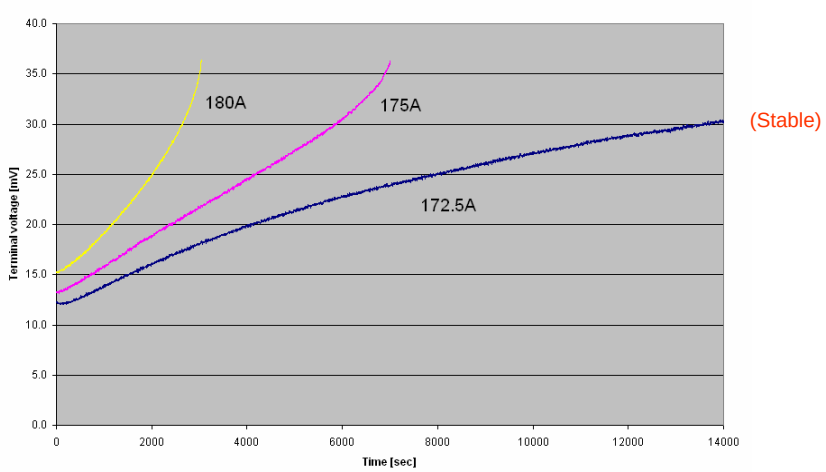

Figure 8-7: Test data for the 1000 hp HTS field coil at 30 Kelvin with various applied currents.

Figure 8-8 shows the test apparatus for the 200 hp BSCCO, HTS coil testing at 30 Kelvin. Figure 8-9 shows typical test data for a single coil test. The quench current for this coil with this cooling method is somewhere between 90 and 92 amps.

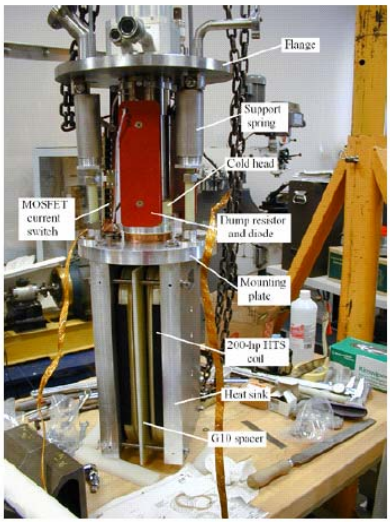

Figure 8-8: Test rig for 200 hp HTS coil testing at 30 Kelvin.

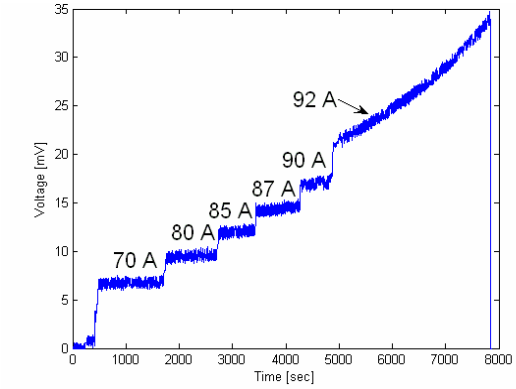

Figure 8-9: Typical test data for a 200 hp HTS coil quench test at 30 Kelvin.

All quench test data shown until now has been with a current induced quench. In these tests, the coil current was increased until voltage instability is obtained. Tests were also conducted to simulate a thermally induced quench produced by a loss of coolant. For these tests, the cryocooler was turned off while the coil was operating with a constant applied current. As the coil warmed up, a quench event was initiated. Figure 8-10 shows typical test results for a 1000 hp motor coil in the 30 Kelvin test rig. Note that the coil voltage increase is quite slow as the time period shown is over the course of 10's of minutes. Figure 8-11 shows measured temperatures in various locations in the 200 hp test rig for a thermally induced quench. Coil temperatures slowly increase (taking minutes) until the coil current is removed and the temperatures come back down. Again, a long period of time is available to detect a problem and take countermeasures.

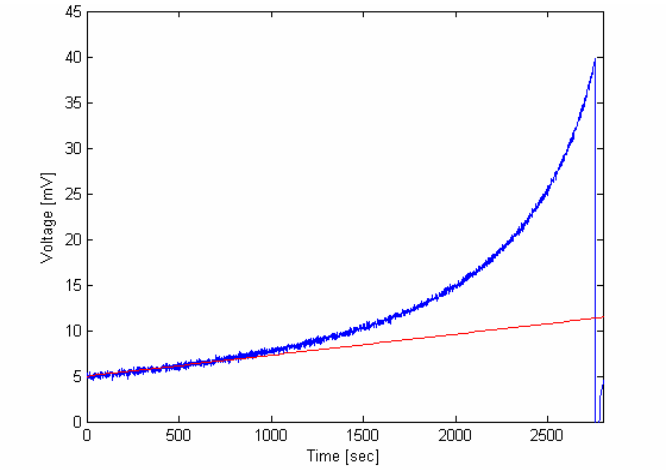

Figure 8-10: 1000 hp BSCCO HTS coil test after the cryocooler is shut down. Constant coil current was maintained until beyond 2500 seconds when the test was shut down.

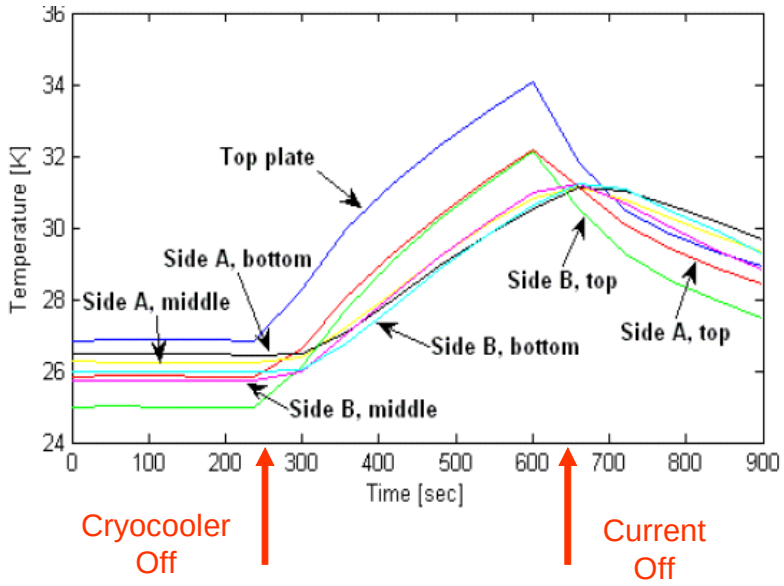

Figure 8-11: 200 hp BSCCO HTS coil test for a temperature induced quench.

The goals of computer modeling of HTS coil quench were to determine the coil temperature distribution and terminal voltage as a function of time in order to provide information for quench detection and protection methods. The simulation should have capability to model the following:

- Current induced quench
- Thermally induced quench
- Impact of localized defects in the coil
- Current sharing between the HTS material and normal conducting stabilizers that are part of the HST wire
- Applicability to any HTS conductor and coil design

The model was developed combined a finite element electromagnetic model and a finite element thermal model that included a representation of the HTS wire voltage drop (throughout the HTS coil) as a function of the applied current, the local magnetic field magnitude and direction, and the coil temperature. The input to the model was wire characterization data which included measured voltage as a function of current, temperature, magnetic field, and magnetic field direction. For any coil current the magnetic field distribution in the coil was determined. From the magnetic field distribution and the wire characterization data the coil loss distribution for any given operating condition of the coil was determined. Knowing the loss distribution and the coil cooling system characteristics the temperature distribution was determined throughout the coil as a function of time. For each time step, the loss distribution was updated based on the known relationship between wire voltage drop, magnetic field, and temperature. The FEA modeling method applies to all operating modes of the coil so it could be used to estimate coil voltage versus current curves in a non-quench condition as well as the voltage and temperature versus time curves for a quench condition.

Figure 8-12 shows the measured V-I curves at 30 Kelvin for the four 1000 hp motor HTS coils along with an FEA model prediction of the coil voltage drop for a 1000 hp motor coil. The FEA predicted voltage is somewhere in the middle of the measured results. Since the HTS wire characteristics are not known for the actual wire used to make these coils, the best that can be expected is for the model results to be roughly the same as the test results, which they are. Wire characterization data used for the model was the result of tests made on a few small samples of HTS wire that were not necessarily from the same batch of wire used to make these coils. Since wire to wire performance variation can be quite large (as witnessed by the differences in voltage drop for the same current for the four different coils in Figure 8-12) the prediction of coil characteristics from a small sample of wire test data is inherently problematic. Consequently, the model results should be viewed as characterizing the general response of the HTS coil to applied current, or, for the quench models, the general response of the HTS coil to a quench event. A successful model should show the same trends as the test data, such as the pre-quench instability regions, and is not expected to exactly predict the coil terminal voltage as a function of time for a given quench scenario.

To illustrate the fact that the model results show the same trends as the test data Figure 8-13 shows test data and computer simulated data of voltage versus time for two different HTS coils. HTS coil test data had similar characteristics for a variety of coils tested so the one shown in this Figure is a typical test result. The model data shows the same characteristics as this typical test data with a region where coil voltage increases linearly with time and a region where the voltage nonlinearly increases with time. The model predicts 10's of minutes of time before the coil voltage starts to increase rapidly with time. This system response is similar to what was observed in coil testing. Other coil operating conditions were also simulated using the quench model and results were used to characterize the performance of HTS coils during a quench.

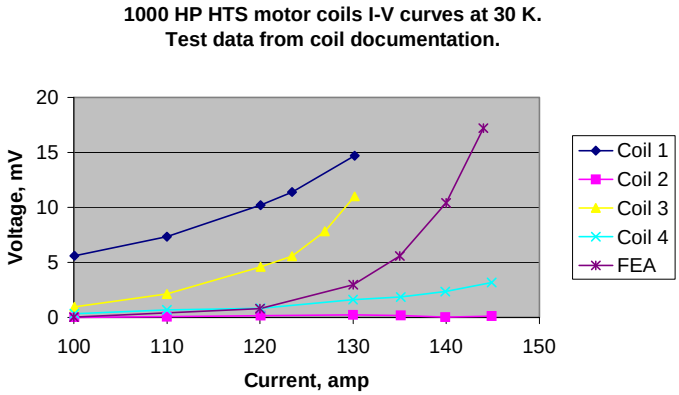

Figure 8-12: 1000 hp BSCCO HTS measured and calculated V-I curves

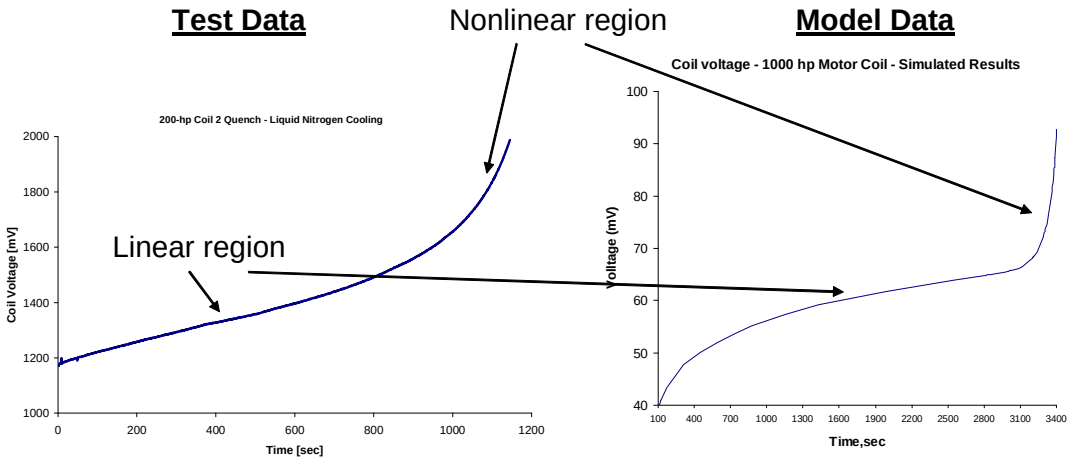

- 200 hp coil test data
- Voltage vs Time
- 1000 hp coil simulation data
- Voltage vs Time

Figure 8-13: HTS coil quench test and model results.

Based upon the test data and model results a quench protection system was developed and tested at ORNL. This system detected the onset of a pre-quench event and then reduced the current in the coil to prevent the event from progressing to a true quench. The detection system did not rely on the coil voltage to detect the onset of pre-quench instability, and was therefore very robust and noise immune.

A number of tests were conducted on the 200 hp and 1000 hp HTS motor coils with liquid nitrogen and 30 Kelvin conduction cooling. The coils were taken from steady state operating conditions into quench a number of times. No damage occurred to any of the coils due to this testing. Based on these test results, as well as the computer modeling of HTS coil quenching, it is believed that the failure of the 1000 hp HTS motor coil (Figure 8-1) was not a true quench event, but rather a failure of the HTS wire, possibly at a joint. The rapid influx of energy in a small region of this coil simply does not match any of the

test data that was taken nor the model results. It is unlikely that the coil failure was due to a classical quench event. It is recommended that HTS coils be fully tested, including excursions into the pre-quench instability region, before installing them in an HTS motor. This type of testing has a better chance of detecting a coil with a localized wire defect before putting it into operation in a motor.

c. Task 6: Publications

Four technical papers were published on HTS coil quench testing and modeling [7-10].

d. Task 6: Conclusions

The concept of the quench event in HTS conductors has now been characterized as follows:

1. In HTS coils, quench (which is defined as the formation and the propagation of the normal zone) is preceded by another phenomenon, which will be referred to as pre-quench instability.
2. Pre-quench instability is by far more important for quench detection and protection than quench itself. We believe that detection and protection could and should occur at the stage of pre-quench instability and that quench should be avoided.
3. The voltage versus time curves for HTS coils in the literature and in the tests we conducted are mainly related to the pre-quench instability; very small parts of the curves if any represent a true quench.
4. If quench detection and protection is done during the pre-quench instability, the speed of the quench propagation (i. e. normal zone) within the coil is irrelevant.
5. In a current induced quench event, pre-quench instability starts when the current (I) slightly exceeds the quench current I_q. Pre-quench instability is comprised of two steps. The first step is a near-linear temperature and voltage increase versus time at each location; the duration of this stage depends on the distribution of the coil voltage drop in the coil and also on the quantity I- I_q and can be minutes, hours and even days. During this first step, current sharing (simultaneous current flow in the superconductor and in the other conductive materials in the HTS wire) is not significant. The second step is an acceleration stage: voltage and temperature rise becomes non-linear with time and current sharing is significant. This second step has a typical duration of a few tens of seconds.
6. Quench starts after the pre-quench instability. During a quench event, the temperature rise is almost adiabatic and the duration of the quench can be estimated from adiabatic considerations.
7. If the superconductor properties are reasonably uniform across the whole coil, then during the pre-quench instability the whole coil essentially behaves as a one-degree-of-freedom system. This degree of freedom can be chosen in many ways, for example, the temperature in *an arbitrary point of the coil* may be used.
8. The most difficult situation for quench detection is the case when a generally good coil has small defects, such as low critical current or low critical temperature in a finite number of locations within the coil. In this case, the amount of the stabilizer becomes critical for quench detection and protection. Theoretically the coil still would go through pre-quench instability, which will last even longer than for a coil

without a defect. But without proper stabilizer, the pre-quench instability caused by the defect would generate practically undetectable voltage or temperature rise in a noisy motor/generator environment. A coil in these conditions does not behave any more as a one-degree-of-freedom system. The initial undetectable pre-quench instability would be followed by an extremely fast local quench, destroying the wire in a fraction of a second. The necessary amount of stabilizer depends on the resolution of the equipment used to measure the coil voltage, and on the wire current, and can be calculated based on these parameters. The general trend is that the larger the current and the lower the resolution, the more stabilizer is needed.

9. A thermally induced quench qualitatively behaves the same way as the current induced quench. A failure or malfunctioning of the cooling system results in temperature increase in the whole coil and consequently in a drop of the quench current, so that at some point the quench current becomes smaller than the operational current and a pre-quench instability starts.
10. The commonly accepted way to characterize the superconducting to normal state transition is to calculate the power constant *n* in the power law relating coil voltage to coil current ($V_{coil} = I_{coil}^{n}$). The properties of the quench event in HTS coils described above are correct for any dissipation law in the superconductor, as long as the transition from the superconducting to normal state is not too sharp, i.e. the constant *n* is less than 50.
11. Quench in HTS coils is strongly dependent upon the cooling system, the HTS wire characteristics, and the coil geometry. The concept of a coil critical current (based on a certain coil voltage at a standard level of μV/cm of wire length) as a benchmark to describe the state of the coil with respect to quench, does not apply well to HTS coils.

The quench mechanism in HTS coils is now well understood and we have demonstrated the validity of the modeling techniques which were developed. The modeling tools are useful when developing wire design, cooling system design, and coil designs for future HTS rotating machinery. They can be used to predict the response of a coil to a quench event based on the amount of stabilizer in the wire, the magnetic field distribution of the coil, and the cooling system's ability to control the rate of rise of temperature during the pre-quench instability period. All of these design attributes can then be optimized to create an HTS coil that will have a long duration pre-quench instability to facilitate detection and coil protection.

Prior to the start of this program, it was anticipated that quench protection in an HTS motor or generator would consist of a voltage-based detection system coupled with a means to dump energy from the HTS coil. The detection system was viewed as extremely technically challenging; its specification required that it detect millivolt level changes in coil voltage in the presence of impressed voltages on the order of tens of volts (required to drive changes in current in the high-inductance HTS field coils) and a large amount of noise, both in the form of exciter ripple voltage (also tens of volts) and large induced voltages from motor drives and other high-power electronic systems. Following the detection of a voltage increase characteristic of a quench, the quench protection system

was to be designed to rapidly de-excite the field winding, quickly removing energy that would otherwise be dissipated in the HTS field coil, with potentially damaging consequences.

Experimental studies of the quench phenomenon using HTS coils from our 200-hp and 1000-hp HTS motors, in combination with analytical studies, has led us to develop a revised understanding of quench in HTS coils and to develop a fresh concept for quench protection/detection. This new concept is much more robust, noise immune and signals an incipient quench long before a quench would occur, leaving plenty of time to de-energize the coil and avoid damage to the coil. One of the many advantages of this concept is that it eliminates the necessity to rapidly dump energy from the field coil and the associated large voltages which might otherwise cause insulation damage. In many cases, upon detection of a problem which might ultimately lead to a damaging coil quench, there will be sufficient time to shut the machine down gracefully, with the HTS field coil being de-energized by the excitation system itself. In the event that a rapid shut-down is required, a dump-resistor system (or equivalent) can be used. However, even in this case, there will be sufficient time to dump the field-winding energy that the dump resistor can be of a sufficiently low value that the resultant voltage transient will not stress the field-winding insulation. During the course of this project task, this new quench-protection system was demonstrated and appears to be practical for use in HTS machines.

9. Task 7: Composite Torque Tubes

a. Task 7: Proposed Activities

The technology innovation of composite torque tubes was implemented in the design of the 1000 hp HTS motor and was successfully demonstrated. The torque tube is a key component that enables a drastic reduction of parasitic heat leak into the cryogenic environment of the superconducting field windings, which leads to a reduction in the size, input power, and cost of the cryogenic refrigeration system. The experience gained in the 1000 hp HTS motor demonstration indicated that the most critical element in the torque tube assembly was the bonded joint between metal and composite in the warm end. Depending on the operating environment, the joint temperature could reach temperatures as high as 100 °C. At such temperature levels, the creep phenomenon in the adhesive and composite structure becomes a serious issue. A better understanding of the creep characteristics of adhesives at these temperatures is necessary for reliable HTS motors to become a reality.

The design requirements for large-scale motors dictate that the shafts (or torque tubes in the case of the HTS motor) sustain constant torque over a life span of approximately 30 years. In order to carry out experiments within a practical time frame, an accelerated test program on creep and a better understanding of fatigue needs to be developed to ensure the longevity and integrity of the torque tube assembly. In this task, creep and fatigue issues at the bonded joint between the metal end fitting and composite torque tube were investigated.

The approach taken was to test adhesives, in an accelerated fashion, for creep characteristics and to chose an adhesive that has the require creep properties that results in long motor life. Fatigue testing was also considered, but after some literature search and the engagement of a fatigue consultant, it was decided that fatigue life testing of adhesive joints was not warranted. In stead, finite element modeling was conducted to determine that fatigue life of the adhesives is not a serious issue. This result is largely due to the fact that the expected fatigue excitation will be an order of magnitude less than the steady state stresses that the torque tube is designed to withstand. In this situation, fatigue life of the torque tube system will be infinite.

b. Task 7: Results Achieved

Reliance Electric introduced composite torque tube technology into HTS electric machinery. Figure 9-1 has a photograph of a composite torque tube sample for the 1000 hp HTS motor. This technology includes an adhesively bonded joint between the composite tube and metal end fitting. This task has two major objectives. The first objective is the characterization of the creep of adhesives selected for the joints. The second objective is the study of the fatigue life of the joints. The adhesives for joints were identified and used in the course of the previous composite torque tube development projects.

There are two torque tubes, one per side of the cold space of the rotor. Each torque tube has two end fittings, and correspondingly two joints. One joint works at cryogenic temperature of ~30 K, the other joint works at an elevated temperature of ~100 C^o. These two joints will be referred to as the cold and the warm joint, correspondingly. The joints are located in the vacuum and therefore are not subjected to any aggressive media. The creep problem is important only for the warm joint while the fatigue should be studied for both cold and warm joints.

Figure 9-1: Composite torque tube sample for the 1000 hp HTS motor. Top flange is removed.

We will discuss first the creep issue. During motor/generator operation the joint is continuously loaded by an operational torque. The bonded joint between the torque tube and metal end fitting is designed to withstand very high torque that will occur in the case of a major motor fault. The design torque is at least 10 times the rated torque of the motor, and it may be even higher than that. The operational torque is therefore a small fraction of the maximal torque for which the joint is designed, but since it is applied all the time the joint potentially may creep. Initially, the adhesive for the torque tube was chosen after a lengthy experimentally based selection process. This adhesive showed excellent properties at cryogenic temperatures. It was used for both ends of the torque tube for the 1000 hp HTS motor demonstration. Unfortunately, experimental evidence that this adhesive creeps at moderate temperatures (about 50 C) was obtained after the rotor had been already built. This creep was not so significant that the motor could not be operated, but it raised the issue of finding a better adhesive for the warm joint. Two high temperature structural adhesive candidates were chosen for evaluation for this task. These adhesives have significant instantaneous strength sufficient to withstand the design

fault loads. However, since the life time of the motor is ~30 years, accelerated testing is necessary to assure that the joints would not fail in creep.

We will now consider the usage of the time-temperature analogy for accelerated testing of adhesives. The time-temperature analogy is a method of extrapolating the test results obtained in short-term tests at an elevated temperature to a long-term adhesive behavior at the operational temperature. It has to be recognized that there is no time-temperature analogy derived from first principles and the only justification of such an analogy is an experiment. Since it is impossible to provide experimental data for the real time to failure, there always will be some risk associated with any time-temperature analogy. The concept adopted in this study is as follows. For electric motors, the motor life is ~ 30 years which is 10^9 sec. From literature it was accepted that the creep test data may be extrapolated by ~ 3 orders of magnitude. Thus we need to obtain a methodology that would work up to a time between 10^6 and 10^7 seconds, that is between 12 days and 116 days. The plan was to conduct four experiments for a chosen stress level. In the first three experiments, temperatures are set up to provide the time to failure somewhere between 10^3 and 10^6 seconds. Using these three experiments, the prediction of failure time for lower temperatures is to be made. According to that prediction, the temperature of the fourth experiment is chosen to provide the time to failure somewhere between 10^6 and 10^7 seconds. If the actual data points of the fourth experiment are within the calculated bounds, then we consider this result as an experimental confirmation of this methodology and will extrapolate the results to the life time of a motor/generator.

Creep testing generally requires multiple samples tested at elevated temperature. In order to reduce the cost and time of testing, a creep test fixture was design and implemented so that multiple samples could be loaded and installed in a laboratory oven thereby reducing the cost and time of testing. Figure 9-2 shows the 32 test fixtures that were designed and built for this testing. Each fixture had one adhesive joint sample loaded into it and the mechanical loading was provided by the spring on the top of the fixture. Load levels were monitored by strain gauges placed between the sample and the fixture base. All 32 fixtures could be loaded into the lab oven at one time so that 32 samples could be tested simultaneously.

Figure 9-2: Creep test fixtures.

A total of 572 samples were tested with a total elapsed test time was 9,197 hours. Test data results for the chosen adhesive at a 750 psi stress level are shown in Figure 9-3. The lower

bound curve also appears in Figure 9-4 along with an equivalent curve for 500 psi stress level for this adhesive. The estimated creep life for this adhesive is above 30 years at 100 degrees C for both of these stress levels.

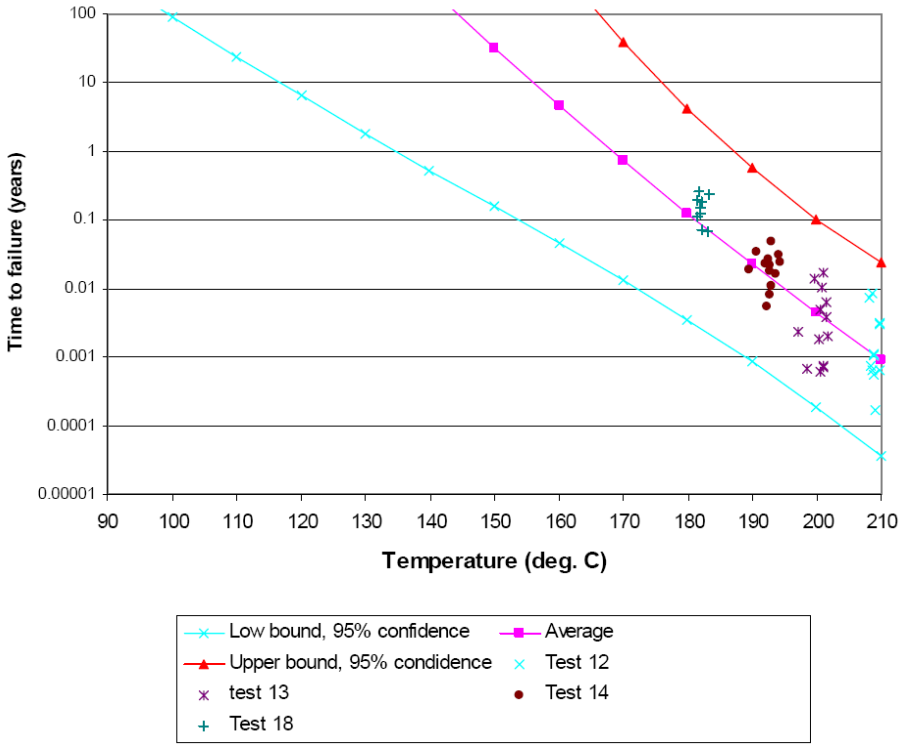

Figure 9-3: Creep test results for 750 psi stress level for one adhesive with 95% confidence intervals shown.

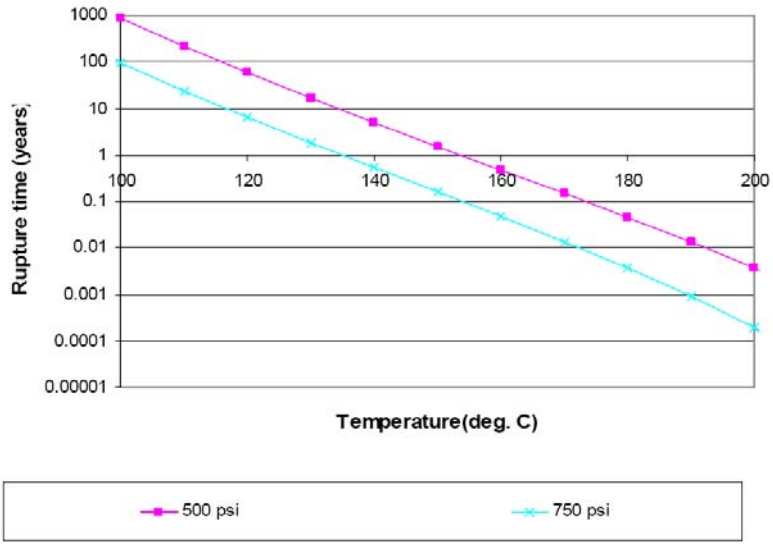

Figure 9-4: Creep lower bound, 95% confidence estimates of time to failure for the chosen adhesive for the composite torque tube joints.

The evaluation of fatigue properties of the joints was done using a fracture mechanics approach. Finite element analysis and closed form solutions were used for calculation of stress intensity factors and energy release rates. The material properties that were used in the analysis were obtained from the literature for adhesives that are similar to those chosen for the torque tube joints. Since the use of the properties of one adhesive to estimate the performance of a different adhesive has inherent inaccuracy, large safety factors were used to partially compensate for these inaccuracies. Fatigue data was found for adhesives that were close to the properties of the adhesives chosen for the torque tube joints. Reliance Electric uses singularity-free joints in the design. These types of joints do not have stress concentrations at the joint surfaces. The results of the fatigue analysis showed that the fatigue life of these singularity-free joints for typical motor applications will be infinite. The assumed maximum amplitude of torque oscillation for this analysis was 100% of the motor rated torque, which would simulate a typical reciprocating compressor load.

One aspect of the joint design that contributes to the very high fatigue life is the fact that the joint steady state design is to continuously carry 10 to 20 times the rated torque of the motor. This large steady state safety factor is necessary so that torque tube failure does not occur during a major motor electrical transient (such as a short circuit at the motor stator terminals).

c. Task 7: Conclusions

A methodology of accelerated creep testing of adhesives for joints of the composite torque tubes of high temperature superconducting (HTS) motor rotors was developed. The methodology provided a prediction of the rupture time in creep of metal-composite joints for a given operational temperature at the warm end of the torque tube. Test data of adhesives showed that the desired 30 year life of the warm-end torque tube joint can be achieved for a joint temperature of 108 degrees C or less.

Reliance Electric uses a singularity free joint (SFJ) design for the torque tubes. Fatigue life of the SFJ was evaluated. It was determined that the SFJ has infinite fatigue life for typical HTS motor rotor designs. The major factor assuring the infinite fatigue life of torque tubes of HTS motors rotors is that the torque tube is designed to withstand very large fault torque, typically exceeding ten times the motor operational torque. Therefore, the cycling loads causing the fatigue are small fractions of the quasi-static joint strength and the stresses in the tubes and joints are below an infinite fatigue life threshold.

10. Task 8: Cryogenic Persistent Current Switch for HTS Windings

a. Task 8: Proposed Activities

The current leads for the HTS field winding coils introduce additional heat leak to the rotor. This heat leak consists of static and dynamic components. The static component is due to parasitic heat conduction and the dynamic component is due to resistive heat generation when the system is energized. Heat leak through conduction occurs when the rotor cryostat is cold. To minimize it, the current leads should have a slender geometry. On the other hand, resistive heat generation primarily represents the I^2R term that occurs in the current leads. Obviously, a larger cross section of the current leads will reduce the heating. The design of current leads is therefore a compromise between these opposite geometric requirements. An optimum current lead system can be designed for a given level of HTS coil current. In other words, for a given operating temperature for the HTS coils, field current, and construction material for the current leads, the cryogenic load from the current leads will be fixed. There is no room for performance improvement unless drastic approaches are taken to change the current lead topology. The total cryogenic load from the current leads including both parasitic and dynamic loads is a few times higher than that from the HTS winding itself. There are obviously incentives to reduce or even eliminate current lead losses.

Running the HTS motor with the field winding in persistent mode offers an opportunity to practically eliminate both parasitic and dynamic cryogenic loads due to the current leads. There have been a number of applications for persistent current switches (PCS's) in superconducting devices. Examples include MRI, SMES, and MAGLEV. For HTS motor applications, since fast response is not a typical design requirement, the construction of a persistent current switch is greatly simplified. This task investigated the various options available for implementing a persistent current switch in the excitation system for the HTS rotor coils with the goal of dramatically reducing the current lead heat load on the rotor cooling system.

The approach taken was to review candidate methods of producing a persistent current switch (PCS) for HTS field windings and select one for test verification of its performance. Based on this performance, an estimate of the heat leak reduction, into the rotor cold space due to the current leads was also made.

b. Task 8: Results Achieved

Under superconducting operating conditions, the resistance of an HTS coil is very low. Thus, if that coil were shorted at its terminal, the L/R (inductance to resistance) time constant of the resultant current decay would be quite long and hence the current would remain essentially constant for a significant period of time. In this case, we can say that the current in the coil persists, and this mode of operation is referred as the *persistent-current mode*.

If the HTS coils could operate in persistent current mode and the current decayed over a period of time much longer than the time in which the HTS coils need to be charged, then the current leads would need to carry current only intermittently. In other words,

excitation would be applied to the coil for a short period of time to charge the coil, the coil would then be shorted through a *persistent-current switch* and the excitation shut off. The excitation would remain off for a long period of time until the coil current decayed to a pre-specified level (e.g. 97% of its initial value), at which point the persistent-current switch would be opened and the coil would be recharged to the desired value. By reducing the rms current that is carried through the excitation leads, the total heat leak into the cold space due to the current leads can be reduced, or, the HTS coil current can be increased to the optimum level for the specific HTS conductor design without a significant impact on heat leak into the cold space. Successful demonstration of a PCS technology is an important step in the optimization of the cold space design for future HTS motors.

The implementation of the PCS in an HTS winding excitation circuit is shown in Figure 10-1 and Figure 10-2. Figure 10-1 shows the configuration of the PCS during HTS field winding charging for a motor field winding excitation system. The PCS remains open while the exciter supplies current to the HTS coils as well as the current through the PCS device. Figure 10-2 shows the persistent mode of the HTS winding with the PCS. Here the exciter is disconnected from the HTS coil/PCS system and the HTS coil current flows through the PCS with a decay in current dictated by the on resistance of the PCS and the HTS coil inductance. The ideal PCS would have zero ohm resistance in the closed, or ON, state and infinite resistance in the open, or OFF state. The ideal PCS would be simple to control and compact in size. It would be capable of handling large currents in the closed state and substantial voltages in its open state. The ideal PCS would be able to change states quickly and would have an infinite life span.

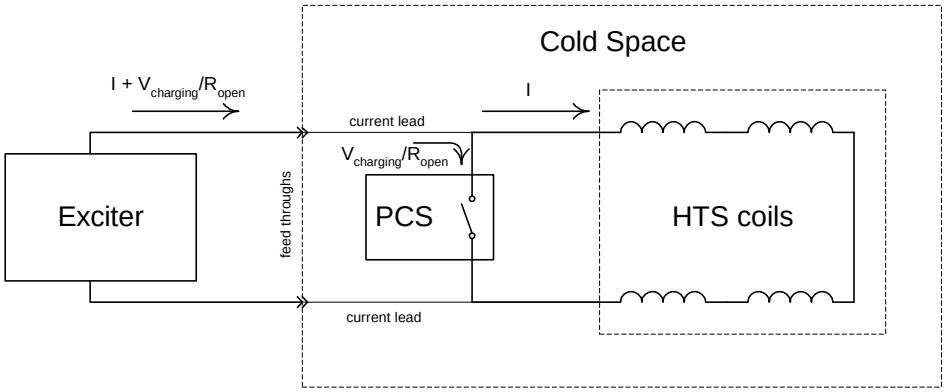

Figure 10-1: Charging mode of a PCS system feeding an HTS coil set.

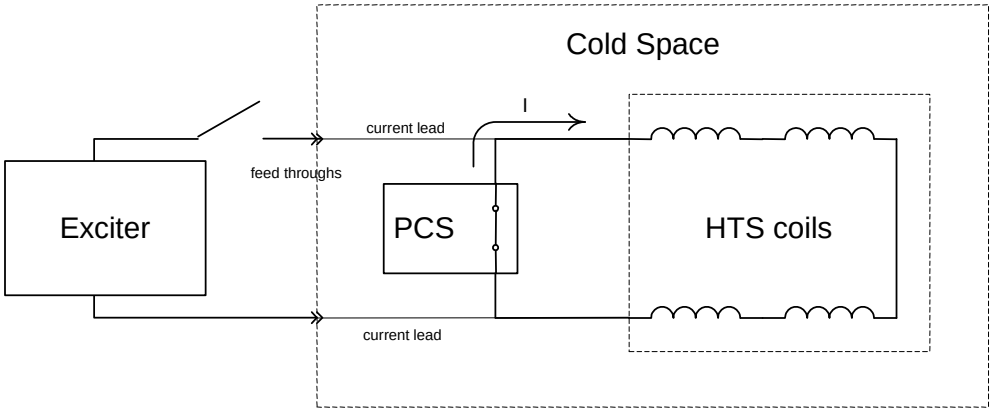

Figure 10-2: Persistent mode of a PCS system feeding an HTS coil set.

In order to draw up a set of design parameters for the PCS, a set of HTS coil parameters were needed. The coil parameters chosen are roughly those of the 1000 Hp HTS motor's field coils. The design parameters for the PCS are listed in Table 10-1.

Table 10-1: Design parameters for a PCS for the 1000 hp motor.

Charging voltage	30	volts
Ripple current	3 %	amps
Maximum ON resistance	0.1	mΩ
Minimum OFF resistance	30	Ω

To illustrate the impact of each of these parameters a set of PCS characteristics based on these parameters can be calculated. For the 1000 hp HTS motor field winding parameters, the duty cycle for current charging of the field winding is 0.13% and the total heat leak into the cold space due to the current leads could be reduced to less than 1% of what is possible with optimized current leads designed for continuous current feed to the HTS coils.

A variety of PCS technologies were investigated and the one chosen was a Metal-Oxide Semiconductor Field-Effect Transistor (MOSFET). Tests were conducted on several MOSFET's at cryogenic temperatures and results were very promising. The final tests consisted of number of parallel MOSFET's that resulted in a current carrying capability in excess of 200 amps with an on and off resistance that exceeded the goals listed in Table 10-1. Tests were conducted in a liquid nitrogen bath. In addition, the MOSFET based PCS was implemented with an HTS coil and liquid nitrogen cooling (see Figure 10-3). It successfully charged and discharged the HTS coil successfully.

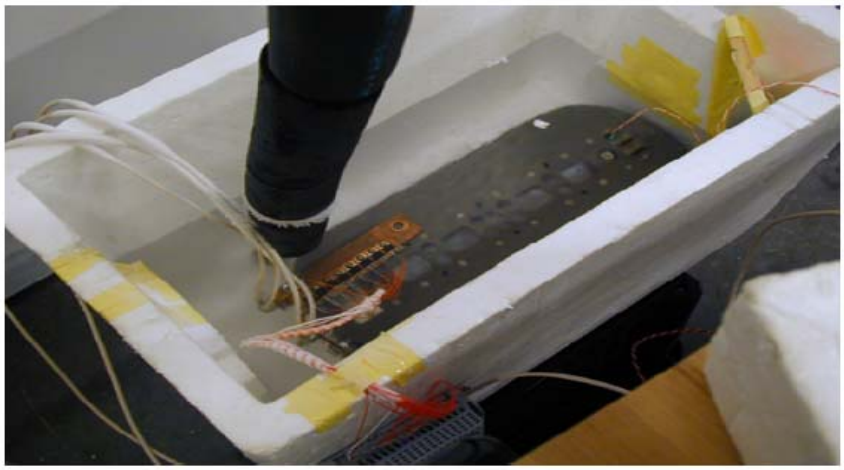

Figure 10-3: A MOSFET based PCS demonstration with a 200 hp HTS motor field coil.

c. Task 8: Conclusions

The MOSFET PCS is the recommended technology for the field windings in future HTS motors. Use of this type of switch offers the potential to reduce the current lead heat leak into the rotor cold space by more than 99%. Tests on MOSFETS at cryogenic temperatures showed that they operate successfully.

11. Conclusions

All project tasks were successfully completed with 7 out of 8 of them resulting in hardware demonstrations that were used to verify computer modeling and analysis concepts. The result of this research will be used to reduce first cost, improve efficiency, and improve the reliability of future HTS rotating machines. The lessons learned from the completion of this project have lead to a series of recommendations for future large HTS motor and motor system design as described in Section 1-c. of this report.

Large HTS motors offer the potential for a 50% volume reduction and a 60% loss reduction compared to large induction motors. However, cost challenges remain for economic viability of large HTS motors for utility and industrial applications. Second generation wire cost must be reduced and a focused effort on reducing the cost of cryocoolers and cryogenic support equipment is also needed in order for HTS motors to compete with large induction motors. In addition, the recent advances in PM material capabilities, with higher energy products and the ability to operate at higher temperatures, will likely result in large PM motors in competition with HTS and induction motors. These PM motors will also be smaller and more efficient than conventional induction motors and will offer stiff competition for HTS motors since PM motors do not require a cryogenic cooling system. The ultimate choice of the best motor for high horsepower applications will come down to the results of cost-benefit analyses made by customers.

12. References

a. Technical Papers

1. Rich Schiferl, Alan Flory, William C. Livoti, Stephen D. Umans, *"High Temperature Superconducting Synchronous Motors: Economic Issues for Industrial Applications."* IEEE, 2006 PCIC Conference, September 2006.
2. C. H. Joshi, C. B. Prum, R. F. Schiferl, D. I. Driscoll, *"Demonstration of Two Synchronous Motors Using High Temperature Superconducting Field Coils, "* IEEE Transactions on Applied Superconductivity, Volume 5, Issue 2, Part 1, Jun 1995 pp 968 – 971.
3. B. Zhang, D. I. Driscoll, V. Dombrovski, *"Construction and Testing of a 1000 hp High-Temperature Superconducting Motor,"* IEEE Petroleum and Chemical Industry Conference Record, Sept. 2002 pp 223 – 228.
4. V. Dombrovski, D. Driscoll, B. A. Shoykhet, S. D. Umans, J. K. Zevchek, *"Design and Testing of a 1000-hp High-Temperature Superconducting Motor,"* IEEE Transactions on Energy Conversion, Volume 20, Issue 3, Sept. 2005 pp. 638 - 643
5. G. Nerowski, J. Frauenhofer, G. Ries, W. Nick, H. W. Neumiiller, *"Advances and Prospects of HTS Rotating Machine Development at Siemens,"* IEEE Power Engineering Society General Meeting, 2004. 6-10 June 2004 pp 2052 - 2055 Vol.2
6. D. Madura, M. Richardson, D. Bushko, G. Snitchler, P. Winn, S. Kalsi, B. Gamble, *"Test Results of a 5000HP HTS Motor,"* IEEE 2002 Applied Superconductivity Conference, August 2002, Houston Texas.
7. S. Umans & B. Shoykhet, *"Quench in High-Temperature Superconducting Motor Field Coils: Experimental Results"*, IEEE, IEMDC Conference, May 2005 – IEEE IAS Transactions, July 2006.
8. S. Umans, B. Shoykhet, J. Zevchek, C.Rey and R. Duckworth, *"Quench in High-Temperature Superconducting Motor Field Coils: Experimental Results at 30 K"*, Invited paper for the IEEE Applied Superconductivity Conference, August, 2006.
9. B.A.Shoykhet, S.D.Umans, *"Quench in High-Temperature Superconducting Motor Field Coils: Reduced-Temperature Modeling of HTS Tapes"*, IEEE Applied Superconductivity Conference, August 2006.
10. B.A.Shoykhet, S.D.Umans**,** *"Quench in High-Temperature Superconducting Motor Field Coils: Computer Simulations and Comparison with Experiments"*, IEEE Applied Superconductivity Conference, August 2006.
11. O.K. Mawardi, *Thin Film Superconducting Synchronous Motor*, US Patent 6,711,422 B2, Mar. 23, 2004.
12. O.K. Mawardi, *Thin Film Superconducting Motor With Magnetically-Quenched Rotor*, US Patent 6,791.229 B2, Sep. 14, 2004.
13. V.S. Vysotsky, et.al., *Stability and Quench Development in Small HTSC Magnet*, Cryogenics 41 (2001) pp. 665-674
14. V.S. Vysotsky, et.al., *Thermal Quench Study il HTSC Pancake Coil*, Cryogenics 40 (2000) pp. 9-17

15. A.L. Rakhmanov, et.al., *Universal Scaling Law for Quench Development in HTSC Devices,* Cryogenics 40 (200) pp. 19-27.
16. A.L. Rakhmanov, et.al., *Quench Development Analysis in HTS Coils by Use of the Universal Scaling Theory*, IEEE Transactions on Applied Superconductivity. Vol. 11, No 1, March 2001, pp. 1824-1827
17. V.S. Vysotsky, et.al., *Stability and Quench Development in HTSC Magnets: Influence of Cooling and Material Properties,CP613,* Advances in Cryogenic Engineering: Proceedings of the Cryogenic Engineering Conference, Vol. 47, pp. 481-488
18. V.S. Vysotsky, et.al., *Influences of Voltage-Current Characteristic Difference on Quench Development in Low-Tc and High-Tc Superconducting Devices (Review), Physica* C 401 (2004), pp.5765.
19. R. Grabovickic, et al, Measurements of Temperature Dependence of the Stability and Quench Propagation of a 20-cm-long RaBiTS YBCO Tape, IEEE Trans Appl Supercond, Vol. 13, 2003.
20. F. Dahlgren, et.al., ARIES-AT Magnet Systems, 2001, on website: http://aries.ucsd.edu/LIB/REPORT/ARIES-AT/FINAL/aat-7-magnet.pdf

b. Presentations

A. Rich Schiferl, "Development of Ultra Efficient HTS Electric Motor Systems", Presentation made to 2004 Annual Superconductivity Peer Review Meeting,Washington, DC, July 27-29, 2004; stored at http://www.energetics.com/meetings/supercon04/pdfs/presentations/c_doe_peer_review_2004_%20final.pdf.
B. Rich Schiferl, "Development of Ultra Efficient HTS Electric Motor Systems", Presentation made to 2005 Annual Superconductivity Peer Review Meeting, Washington, DC, August 2-4, 2005; stored at http://www.energetics.com/meetings/supercon05/pdfs/presentations/schiferl.pdf.
C. Rich Schiferl, "Development of Ultra Efficient HTS Electric Motor Systems", Presentation made to 2006 Annual Superconductivity Peer Review Meeting, Washington, DC, July 26, 2006; stored at http://www.energetics.com/meetings/supercon06/pdfs/SPI%20Session/Wednesday%20presentations/04_Rockwell_HTS_Motor.pdf.
D. Rich Schiferl, "Development of Ultra Efficient HTS Electric Motor Systems", Presentation made to 2007 Annual Superconductivity Peer Review Meeting, Washington, DC, August 8, 2007; stored at http://www.energetics.com/supercon07/pdfs/Reliance_Dev_Ultra-Efficient_HTS_Motor_Sys.pdf

13. Appendix - Nomenclature

- AC – Alternating Current
- BSCCO - Bismuth-Strontium-Calcium-Copper-Oxide superconducting material. Often called first generation HTS material.
- CRADA – Cooperative Research and Development Agreement
- CSI – Current Source Inverter
- DC – Direct Current
- DoE – U. S. Department of Energy
- FEA – Finite Element Analysis
- hp – Horsepower
- HTS – High Temperature Superconducting
- LTS – Low Temperature Superconductors
- MAGLEV – Magnetic Levitation
- MOSFET - Metal-Oxide Semiconductor Field-Effect Transistor
- MRI – Magnetic Resonance Imaging
- MV – Medium Voltage, generally speaking these are rms voltages in the range of 1000 volts to 6600 volts.
- NIST – National Institute of Standards and Technology
- ORNL – Oak Ridge National Lab
- PCS – Persistent Current Switch
- PIT – Powder in Tube
- PM – Permanent Magnet
- rms – root mean squared
- SCIM – Superconducting Induction Motor
- SFJ – Singularity Free Joint
- SHE – Selective Harmonic Elimination
- SMES – Superconducting Magnetic Energy Storage
- TYCOB – Two Year Cost of Ownership Benefit
- VSI – Voltage Source Inverter
- YBCO - Yttrium-Barium-Copper-Oxide superconducting material. Often called second generation HTS material.
- 2G – Second generation. Often used to refer to YBCO material, especially when referenced to HTS wire.